A Diagnostic and Modeling Study of the Monthly Mean Wintertime Anomalies Appearing in a 100-Year GCM Experiment

MINGFANG TING

Cooperative Institute for Research in Environmental Sciences, University of Colorado, Boulder, Colorado

NGAR-CHEUNG LAU

Geophysical Fluid Dynamics Laboratory/NOAA, Princeton University, Princeton, New Jersey

(Manuscript received 9 June 1992, in final form 21 December 1992)

ABSTRACT

The nature of simulated atmospheric variability on monthly time scales has been investigated by analyzing the output from a 100-year integration of a spectral GCM with rhomboidal wavenumber 15 truncation. In this experiment, the seasonally varying, climatological sea surface temperature was prescribed throughout the world oceans. The principal modes of variability in the model experiment were identified by applying a rotated empirical orthogonal function (EOF) analysis to the Northern Hemisphere monthly averaged 515-mb geopotential height for the winter season (November through March). The individual leading spatial modes are similar to the observed north–south dipoles over the North Atlantic and North Pacific, as well as wavelike patterns in the Pacific/North American and Northern Asian sectors.

Quasigeostrophic geopotential tendencies forced by synoptic-scale (2.5–6 day) eddy vorticity and heat fluxes were computed for those months when the individual EOF modes are particularly active. The composite patterns of the eddy-induced tendencies were compared with the corresponding monthly mean anomaly patterns. It is seen that the forcing due to eddy vorticity transports exhibits a distinctive barotropic character, and reinforces the monthly averaged geopotential height anomalies throughout the tropospheric column. On the other hand, the eddy heat fluxes lead to dissipation of the monthly mean height anomalies in the upper troposphere, and enhancement of the height anomalies in the lower troposphere. Hence, the eddy heat fluxes exert a strong impact on the baroclinic component of the circulation by destroying the concurrent local monthly mean temperature and geopotential thickness anomalies. The above relationships based on model data are in agreement with the corresponding observational results.

A linear stationary wave model was then used to mimic the individual EOF modes appearing in the GCM experiment, and to diagnose the relative importance of different types of forcing in the generation of such modes. As suggested by the tendency calculations, the transient eddy forcing due to heat fluxes was parameterized as a thermal diffusion mechanism in the stationary wave model. When the model was linearized about the climatological zonally averaged basic state, it failed to reproduce the EOF patterns appearing in the GCM experiment. However, when the same model was linearized about the zonally varying GCM climatology, the response to the total forcing (which includes vorticity fluxes by eddies on submonthly time scales, diabatic heating, and nonlinearity in those months when the individual EOF modes are active) bears a considerable resemblance to the corresponding anomaly patterns in the GCM. By evaluating the individual contributions of each of the three forcing mechanisms to the total linear model solution, it is concluded that the transient eddy vorticity fluxes exert the strongest influences. The response to nonlinear effects is negligible, while the forcing due to diabatic heating is weak and acts in opposition to the anomaly patterns in the upper troposphere. The forcing associated with vorticity fluxes by synoptic-scale transient eddies accounts for approximately half of the total vorticity forcing due to all submonthly fluctuations.

Both the tendency calculations and the stationary wave model results indicate the crucial role of vorticity transports by transient eddies. The linear model solutions also illustrate the importance of incorporating the climatological stationary waves in the basic state. These findings hence suggest that the monthly mean anomalies in this GCM experiment are intimately linked to barotropic interactions between transient fluctuations of different time scales, and between the monthly mean anomalies and the climatological stationary waves.

1. Introduction

Since the early work of Walker and Bliss (1932), much progress has been made in our empirical understanding of geographically fixed oscillations (or "teleconnection" patterns) in the extratropical atmosphere (e.g., Kutzbach 1970; van Loon and Rogers 1978; Wallace and Gutzler 1981; Horel 1981 and others). Most of these patterns have more pronounced signatures in the winter (Barnston and Livezey 1987). Blackmon et al. (1984a,b) studied the behavior of atmospheric fluctuations with different time scales, and

Corresponding author address: Dr. Mingfang Ting, Department of Atmospheric Sciences, University of Illinois at Urbana–Champaign, 105 S. Gregory Avenue, Urbana, IL 61801.

concluded that the geographically fixed teleconnection patterns are evident only on time scales of a month and longer. A deeper understanding of the nature of the low-frequency fluctuations in the middle and upper troposphere is crucial for advancing our skill in long-range weather prediction, since they are closely related to short-term climate fluctuations at the surface (Klein 1983).

The origin and maintenance of the observed extratropical low-frequency anomalies has also been a subject of considerable theoretical and modeling interest during the past decade. The notable correlation between the low-frequency pattern indices and the tropical precipitation anomalies (Horel and Wallace 1981) indicates a potential role for external tropical forcing, such as sea surface temperature (SST) anomalies associated with El Niño events. General circulation model (GCM) experiments with prescribed El Niño–like SST anomalies had some success in reproducing the observed seasonal mean extratropical anomalies accompanying such events (e.g., Shukla and Wallace 1983; Blackmon et al. 1983; Geisler et al. 1985; Lau 1985). Linear modeling results of Rossby wave dispersion from a steady tropical heat source (Hoskins and Karoly 1981; Simmons 1982) also seem to support a role for tropical heating.

Lau (1981) reported that low-frequency oscillation patterns were also detected in a GCM integration without any SST anomalies. It is hence conceivable that low-frequency variability could be generated both internally within the atmosphere and externally by anomalous SST forcing. One candidate for the internal mechanisms is the barotropic instability of the zonally asymmetric background flow (Simmons et al. 1983; Branstator 1985a,b; Branstator 1990). The studies of Zhang (1988) and Anderson (1991) revealed further complications of the barotropic instability problem. However, the relevance of some of the unstable modes to the low-frequency patterns in the observed atmosphere is still discernible in the latter studies.

Lau (1988) and Lau and Nath (1991, hereafter referred to as LN) reported well-defined relationships between variability of the observed monthly mean circulation and that of the eddy transports by high-frequency transients in the vicinity of the wintertime storm tracks. In these observational studies, the quasigeostrophic height tendency due to transient vorticity fluxes reinforces the monthly mean circulation anomalies throughout the troposphere. The transient heat transport, on the other hand, tends to dissipate the upper-tropospheric circulation, and enhance the lower-tropospheric geopotential anomalies. It is also found in the modeling results of Held et al. (1989) that the response of a GCM developed at the Geophysical Fluid Dynamics Laboratory (GFDL) to El Niño SST anomalies is dominated by the effects of midlatitude transient vorticity fluxes; the effect of tropical heating is weaker, although of the same sign. By diagnosing the low-frequency anomalies in a perpetual January integration of the NCAR Community Climate Model, Branstator (1992) demonstrated the importance of transient eddy vorticity fluxes. He also emphasized the role of resonance modes of the zonally varying climatological background flow in maintaining the low-frequency anomalies. All the above works indicate that the complex interactions among the high-frequency eddies, the low-frequency anomalies, and the zonally varying climatological mean flow may account for a substantial fraction of the low-frequency atmospheric variability. Many questions remain to be answered, however. Among these questions are the following.

- Are linear dynamics sufficient for describing the low-frequency anomalies? Or are these anomalies essentially governed by nonlinear processes?
- To what extent are the findings based on tendency considerations (Lau 1988; LN) applicable to an understanding of the steady-state response of observed and GCM atmospheres to eddy forcing?
- In what way does the zonally varying basic state influence the response to various forcings? What are the relative roles of normal-mode instability, resonance, and other processes in this context?
- What is the role of midlatitude heating associated with variability of the storm tracks?

The purpose of this paper is to address some of the above issues by analyzing the monthly mean anomalies in a 100-year GCM experiment with a fixed seasonal cycle. The same climatological seasonal SST conditions were imposed at the lower boundary in all years of the experiment. Thus, there is no external source of variability other than the seasonal cycle.

Recurring anomaly patterns in the model atmosphere were identified by applying a rotated empirical orthogonal function (EOF) analysis to the Northern Hemisphere monthly mean 515-mb geopotential height. Tendency calculations based on the quasigeostrophic potential vorticity equation were performed on the GCM data in a similar manner to that described in LN. A novel aspect of the present model diagnosis is the inclusion of the tendency due to diabatic heating. These tendency results serve to illustrate the local nature of various forcings, but they do not provide information on the remote influences of such forcings, the advective role of the background flow, or the pattern and magnitude of the steady-state response to each type of forcing. The stationary wave models described in Ting and Held (1990) were developed with precisely the latter issues in mind. These models are formulated as the exact linear counterparts of the GCM. If the linear model, when subjected to the sum of all anomalous forcing mechanisms incorporated in the full GCM, is able to reproduce the low-frequency anomaly patterns appearing in that GCM, one can then examine the linear response to a particular component of the anomalous forcing (such as eddy fluxes, forcing due

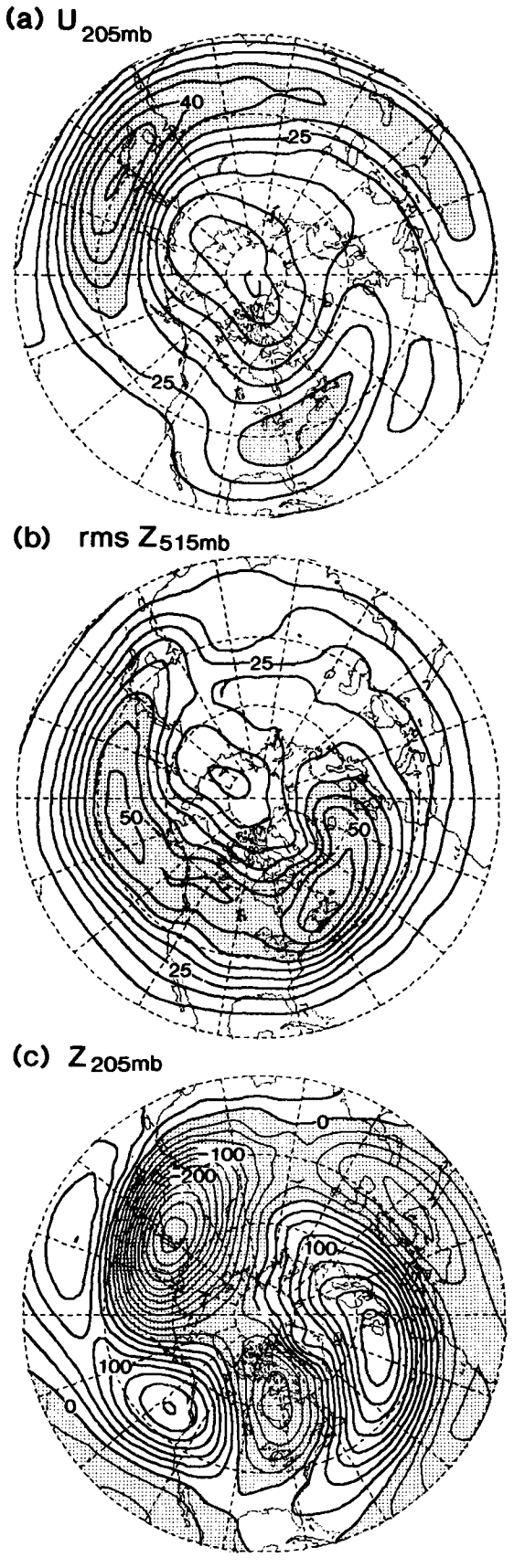

to change in zonal-mean zonal flow, or diabatic heating) separately, so as to distinguish the contributions of these individual processes to the total GCM response. This model diagnostic technique has been successfully implemented to diagnose the climatological stationary waves (Nigam et al. 1986, 1988), as well as the forced low-frequency circulation anomalies (e.g., Held et al. 1989; Ting and Held 1990; Ting 1991).

This paper is organized as follows. A brief description of the GCM experiment and the model climatology is given in section 2. The principal modes of variability in both the simulated circulation and the accompanying transient eddy forcing are presented in section 3. The formulation and results of the quasigeostrophic tendency calculations are documented in section 4. A brief description of the linear stationary wave model and a detailed account of the solutions of this model are given in section 5. The main findings of this study are summarized in section 6.

2. GCM experiment and model climatology

The GCM experiment examined in the present study is part of an initiative to enhance collaboration among GFDL and university investigators in the diagnosis of regional climate variations on the basis of model datasets. This study is based on the last 100 years of a 110-year model integration. The model is a standard version of the spectral atmospheric GCM developed and maintained by the Climate Dynamics Project at GFDL. The horizontal variations of the model fields are represented by spherical harmonics using a rhomboidal truncation at wavenumber 15 (R15), which corresponds to a Gaussian grid with a resolution of 7.5° in longitude and 4.5° in latitude. There are nine unevenly spaced sigma levels in the vertical. Finite differences are used to compute the vertical advection terms. The SST field has been constrained to evolve through identical annual cycles, as determined by climatological observations. Hence, there is no interannual variation in the SST condition throughout the world oceans. Other boundary conditions, such as sea ice, continental snow cover, land surface temperature, and soil moisture, are predicted by the model physics. The model also predicts cloud formation. There is no diurnal variation in the model. More detailed information on this model has been given by Gordon and Stern (1982) and Manabe et al. (1978).

FIG. 1. Northern Hemisphere wintertime (November through March) climatology of the 100-year GCM experiment. (a) Zonal wind component at 205 mb, contour interval 5 m s^{-1}. Values larger than 30 m s^{-1} stippled. (b) Root-mean square of bandpass-filtered geopotential height at 515 mb, contour interval 5 m. Values greater than 40 m stippled. (c) Zonally asymmetric component of geopotential height at 205 mb, contour interval 20 m. Negative values stippled. In these and all following polar stereographic maps, the latitude circles are shown at intervals of 20°, with the outmost circle corresponding to 20°N.

This paper is primarily concerned with the origin and maintenance of the Northern Hemisphere wintertime monthly mean anomalies. These anomalies are defined as deviations from the model climatology for the corresponding calendar month. The northern winter months are taken to be November, December, January, February, and March. The model climatology for the five-month winter season (as computed using the data for a total of 500 winter months) is displayed in Fig. 1. The climatology for individual calendar months exhibits only minor differences from the seasonal climatology shown here. The model fields may be compared with their observational counterparts, such as those compiled by Schubert et al. (1990a,b). The pattern for the zonal wind at 205 mb (Fig. 1a) is characterized by two distinct elongated maxima at about 40°N and off the east coasts of the Asian and North American continents. Both the Asian and North American jet streams in the model atmosphere are weaker than the corresponding features in the observations. However, the geographical locations of the jet streams are simulated well by the model. The distribution of the root mean squares of bandpass-filtered geopotential height at 515 mb is shown in Fig. 1b. The time filter used here has been described by Blackmon and Lau (1980), and retains fluctuations with periods between 2.5 and 6 days. Maxima in the rms geopotential height field depict the preferred sites of synoptic-scale activity, and are good indicators of the locations of the wintertime storm tracks. In agreement with observations, the principal maxima in synoptic-scale variability are located downstream and slightly poleward of the two wintertime jet streams. The extrema in Fig. 1b are 7–8 m weaker than the corresponding observed values (e.g., see Fig. 8a in Blackmon and Lau 1980). Although the zonal wind over the North American seaboard is about 15 m s^{-1} weaker than its counterpart over eastern Asia, the storm track over the Atlantic is noticeably stronger than that over the Pacific. The separation between the Atlantic and Pacific storm tracks is much less evident in the model atmosphere (Fig. 1b) than in the observation. This discrepancy has also been noted in a perpetual January GCM experiment by Kushnir and Lau (1992). The departure from zonal symmetry of the climatological geopotential height at 205 mb is mapped in Fig. 1c. This pattern exhibits the familiar wavenumber two structure in the extratropics, with troughs over eastern Asia and eastern North America, and ridges over the Gulf of Alaska and eastern Atlantic/northern Europe. Except for the weaker amplitude of the North American trough in the model atmosphere, the gross features of the climatological stationary waves in Fig. 1c compare well with the observations.

3. Principal modes of variability in the GCM

The recurrent circulation anomalies have been identified by performing a rotated empirical orthogonal function analysis on the monthly averaged 515-mb height field. The database for this analysis consists of simulated height data for 500 winter months, with the spatial domain extending from 20.25° to 74.25°N. The correlation coefficient matrix was constructed using the time series at 132 grid points within the latter domain. The locations of these grid points have been selected on the basis of equal-area considerations. The climatological seasonal cycle has been removed from the time series prior to the EOF analysis. The spatial patterns of the leading four EOFs are illustrated in Fig. 2, which shows the temporal correlation coefficients between the time coefficients for individual EOFs and the monthly mean 515-mb geopotential height throughout the Northern Hemisphere. These four EOFs (hereafter referred to as EOF1, EOF2, EOF3, and EOF4) explain 7.3%, 5.8%, 5.0%, and 4.9% of the total variance, respectively.

The most prominent feature in EOF1 (Fig. 2a) is the north–south dipole over the North Atlantic, with centers of action over Greenland and along 35°–40°N, and with the nodal line being almost coincident with the climatological axis of the Atlantic storm track (see Fig. 1b). This pattern bears some resemblance to the observed "Atlantic" pattern documented by Hsu and Wallace (1985, Fig. 4) and the North Atlantic Oscillation described in Barnston and Livezey (1987, Fig. 2). A similar dipole straddles the North Pacific storm track in the pattern for EOF2 (Fig. 2b), which is similar to the observed "Pacific" pattern reported in Hsu and Wallace (1985, Fig. 8), and is representative of blocking ridges over the Aleutians (e.g., Mullen 1987, Fig. 8a). Both EOF1 and EOF2 exhibit a certain degree of zonal symmetry. EOF3 (Fig. 2c) shows a more wavelike structure, with a well-defined wave train extending from the subtropical Pacific across the North American continent. The anomaly centers over the North Pacific, western U.S./Canada border, and the southeastern United States correspond well with the centers of action accompanying the observed Pacific/North American pattern (Wallace and Gutzler 1981, Fig. 16; Barnston and Livezey 1987, Fig. 3). The main centers of EOF4 (Fig. 2d) span the Eurasian landmass, in a configuration similar to that associated with the observed Northern Asian pattern (Esbensen 1984, Fig. 6; Barnston and Livezey 1987, Fig. 6). The main focus of this paper is on the nature of EOF1 and EOF2. Brief descriptions of the corresponding results for EOF3 and EOF4 will be offered when necessary.

In this study, the circulation changes accompanying a given EOF mode are described using composite charts. The average of a selected variable over those 50 months (i.e., one-tenth of a 500-month sample) with the most negative time coefficients for the EOF under investigation is subtracted from the corresponding average over the 50 months with the most positive time coefficients. Figure 3 displays such a set of composite patterns associated with EOF1 (left panels) and

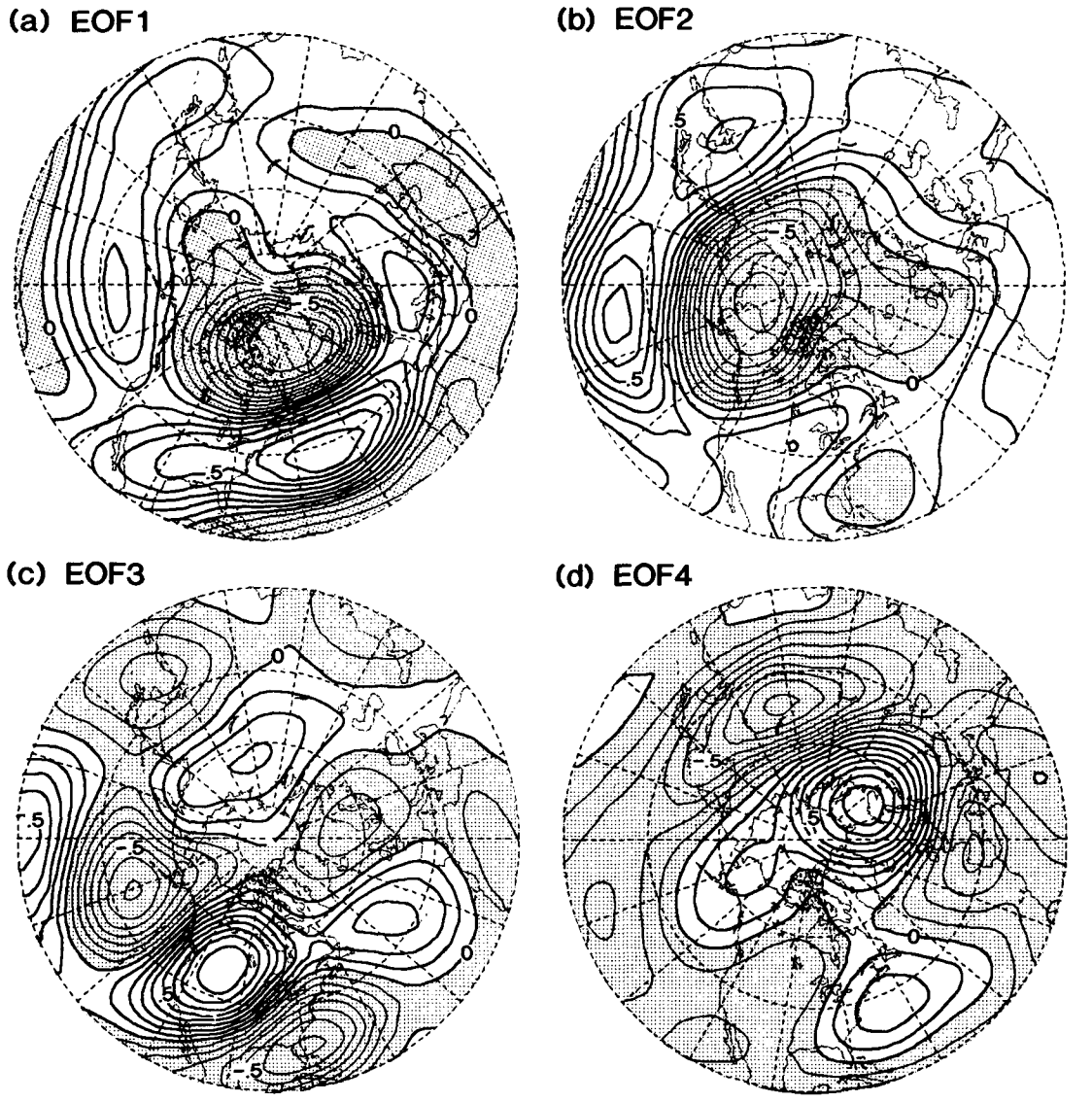

FIG. 2. Temporal correlation coefficient between the monthly mean 515-mb height at individual grid points and time coefficients of the leading rotated empirical orthogonal functions of the same field. (a) EOF1, (b) EOF2, (c) EOF3, and (d) EOF4. Contour interval 0.1. Negative values stippled.

EOF2 (right panels). The variables selected here are the geopotential height at 205 and 940 mb, and the rms of bandpass-filtered height at 515 mb. By comparing Fig. 2a with Fig. 3a, and Fig. 2b with Fig. 3b, it is evident that the composite procedure captures the essential features of the two leading EOFs. The composite charts also provide additional information on the typical amplitude and vertical structure of the anomalies in periods when a given EOF is prominent. The positive phase of EOF1 is characterized by a deep low center over Greenland, a zonally elongated belt of above-normal heights at approximately 45°N, strong anomalous westerlies between these two anomaly centers, enhanced synoptic-scale variability along the 55°–70°N zone over the North Atlantic, and reduced transient activity in regions farther south. Analogous circulation changes are simulated over the North Pacific in association with EOF2. The close relationship between the monthly mean anomalies and the bandpass-filtered rms statistics is suggestive of strong interactions between the low- and high-frequency components of the circulation. The horizontal structure of the anomalous height patterns at 940 mb (middle panels in Fig. 3) is essentially the same as that at 205 mb. The typical amplitudes of the height anomalies in the lower troposphere are approximately one-third to one-half of those near the tropopause. The 940-mb pattern for EOF1 (Fig. 3c) bears some resemblance to the observed

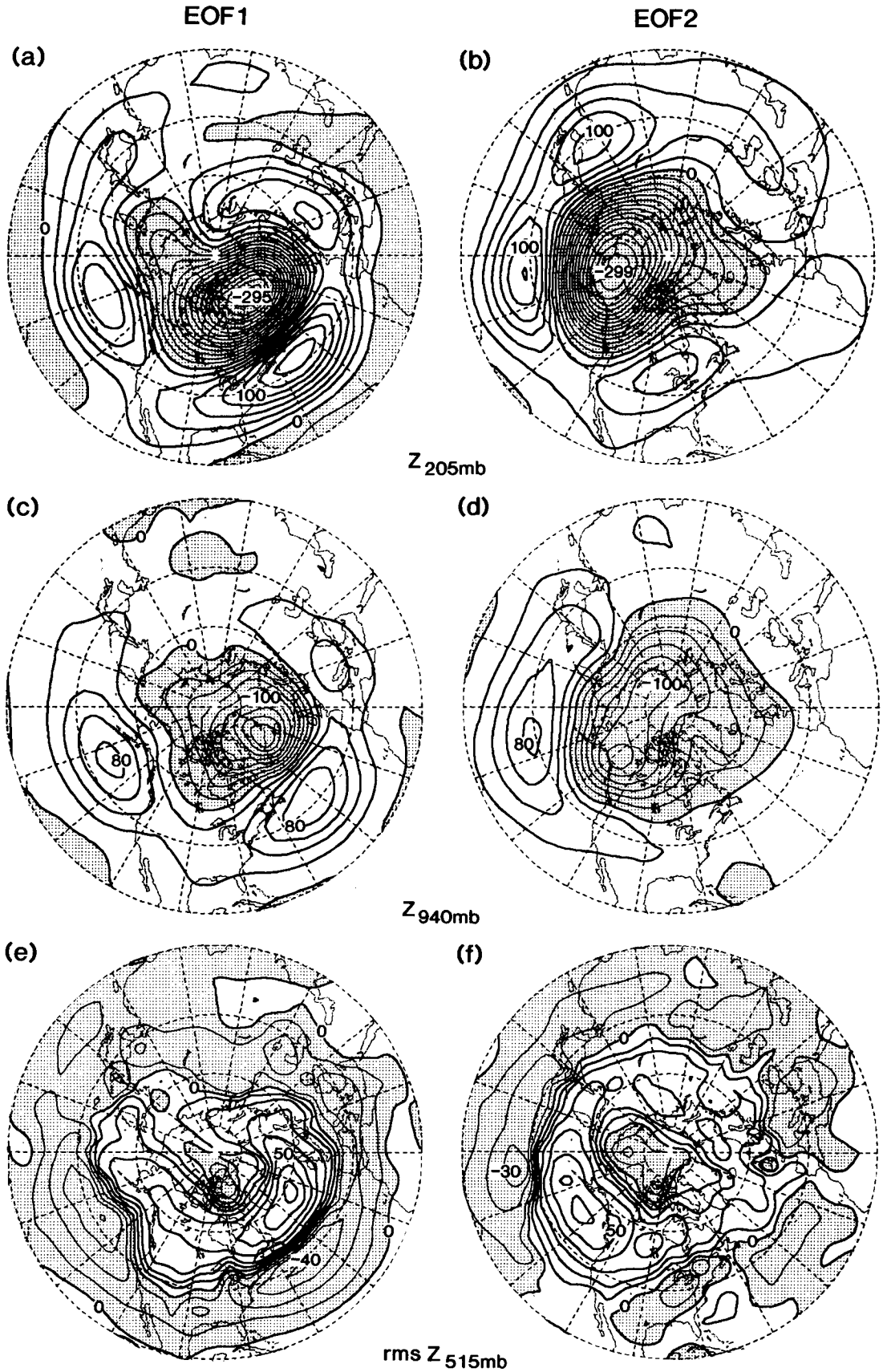

FIG. 3. Composite patterns of geopotential height at 205 mb (panels a, b) and 940 mb (panels c, d), and of root-mean square of bandpass-filtered 515-mb height (panels e, f), as constructed on the basis of the time coefficients for EOF1 (left panels) and EOF2 (right panels). Contour intervals are 20 m in (a)–(d), and 10 m in (e)–(f). Negative values stippled.

anomalous sea level pressure pattern associated with the temperature seesaw between Europe and Greenland (van Loon and Rogers 1978).

The composite height anomaly distributions for EOF3 and EOF4 (not shown) are similar to the spatial patterns shown in Figs. 2c,d. The composite charts of rms of bandpass-filtered height for EOF3 and EOF4 exhibit more small-scale features, partly as a result of the more wavy structure of the monthly mean circulation associated with these two modes. The spatial relationships between the anomalous monthly mean zonal wind and the synoptic-scale eddy activity for EOF3 and EOF4 are similar to those discerned in the two leading EOFs.

In order to explore the relationship between the variability of the monthly mean circulation and that of the synoptic-scale eddy activity, composite charts of the eddy forcing associated with vorticity and heat transports by the high-frequency transient disturbances have been constructed for each EOF. Eddy effects due to fluctuations that encompass all time scales between a day and a month (hereafter referred to as submonthly

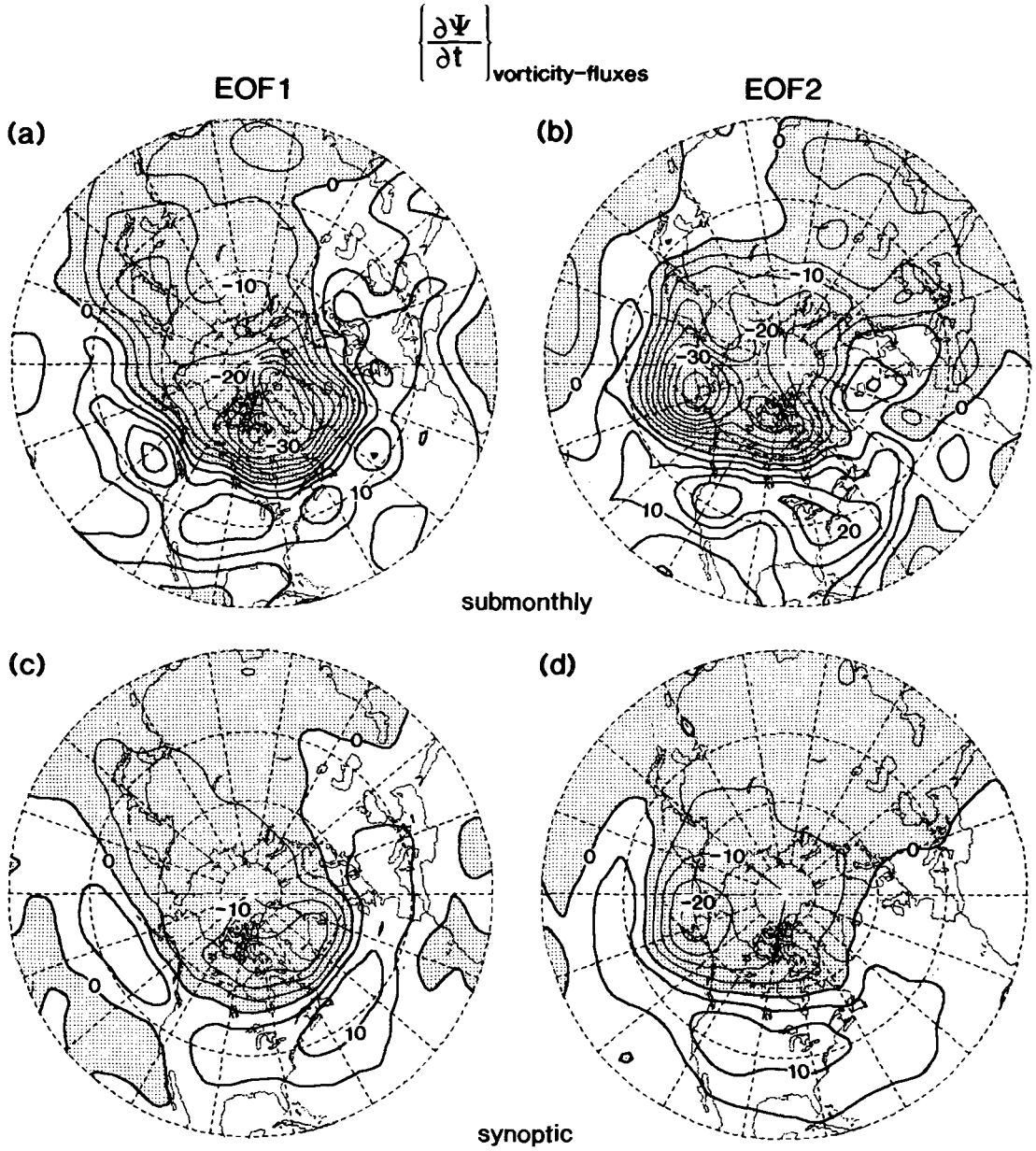

FIG. 4. Composite patterns of 205-mb streamfunction tendency due to convergence of vorticity fluxes by all submonthly eddies (panels a, b), and by bandpass-filtered eddies (panels c, d), as constructed on the basis of the time coefficients for EOF1 (left panels) and EOF2 (right panels). Contour interval 5 $m^2 s^{-2}$. Negative values stippled.

eddies), and those associated with 2.5–6-day time scales retained by the bandpass filter (hereafter referred to as synoptic eddies), are considered separately. The eddy vorticity and thermal forcing due to submonthly fluctuations in each month were calculated as residuals of the full GCM equations upon substitution of the monthly mean model data. The corresponding forcing due to synoptic eddies was obtained by computing the convergence of the vorticity and heat fluxes using bandpass-filtered data. The forcings due to eddy fluxes and diabatic heating will be used to obtain quasigeostrophic geopotential height tendencies (section 4) and linear solutions of a stationary wave model (section 5). In the present section, we shall first describe briefly the forcing terms. The horizontal fields shown here are for data values at isobaric surfaces, as obtained by linear interpolation of the original values at sigma surfaces.

Figure 4 shows the composites for EOF1 and EOF2 of the 205-mb streamfunction tendency due to vorticity transports. These tendencies have been obtained by computing the inverse Laplacian of the convergence of eddy vorticity fluxes associated with submonthly eddies (upper panels) and synoptic eddies (lower panels). A similar computation has been performed by Lau [1988, Eqs. (1)–(2)] using observational data. A dipolelike pattern prevails over the North Atlantic for the EOF1 composites. The streamfunction forcing for the EOF2 mode is characterized by a center over the Bering Sea, and an extremum with the opposite polarity in the eastern Pacific/North American sector along 40°N. The tendency charts in Fig. 4 exhibit a notable spatial resemblance with the corresponding patterns for monthly mean height anomalies in Figs. 3a,b, thus indicating a strong reinforcement of the low-frequency circulation changes by the transient eddies through vorticity transports. The streamfunction tendency due to submonthly eddies is qualitatively similar to that due to synoptic eddies. The synoptic disturbances account for approximately half of the forcing associated with fluctuations with submonthly time scales.

The composites for EOF1 and EOF2 of the 830-mb temperature tendency due to submonthly eddies (upper panels) and diabatic heating (lower panels) are shown in Fig. 5. For the positive phase of EOF1, the eddy thermal forcing (Fig. 5a) is characterized by warming over the Davis Strait and along 55°N over the North Atlantic, and cooling along 45°N over the North Atlantic and near the Arctic coasts of northern Europe and Russia. Comparison of this pattern with the composite chart of rms of bandpass-filtered height (Fig. 3e) reveals that the warming and cooling noted above take place poleward and equatorward of the region of above-normal synoptic-scale activity, respectively. The enhanced poleward heat transport across this active region would lead to a reduction of the local meridional temperature gradient, and through the thermal wind relationship, a weakening of the anomalous westerlies in the upper troposphere. A similar set of relationships among the temperature tendency, the anomalous storm track, and the anomalous zonal wind also holds for EOF2 (see Figs. 5b, 3f, and 3b). The results for the temperature tendency due to synoptic eddies (not shown) are very similar to those for the submonthly eddies, again with the bandpass fluctuations accounting for approximately half of the total eddy forcing.

The temperature tendency due to total diabatic heating is characterized by a north–south dipole over the North Atlantic and North Pacific in the EOF1 and EOF2 composites (Figs. 5c,d), respectively. These features correspond well with the oceanic portion of the dipolar pattern in the rms of bandpass-filtered height for the same EOF modes (see Figs. 3e, f). This relationship indicates that variations in diabatic heating in the model extratropics are essentially governed by the amount of latent heat release accompanying the passage of precipitating cyclone systems along the oceanic storm tracks, with above-normal levels of synoptic-scale activity being associated with heavier precipitation and enhanced latent heating, and vice versa. The anomalous heating outside of the extratropical North Atlantic and North Pacific is uniformly weak. The tropical zone (not shown) is void of any noticeable extrema in the diabatic heating field. Hence, in the absence of nonseasonal SST variations in the present experiment, the leading modes of variability appearing in the extratropical model atmosphere do not seem to be linked to any tropical influences.

The anomalous thickness field, as inferred from the composite charts for the 205- and 940-mb heights in Fig. 3, generally exhibits a negative spatial correlation with the temperature tendencies displayed in Fig. 5. Hence, both the eddy heat flux convergence and diabatic heating act to offset the anomalous monthly mean temperature gradients associated with the EOF1 and EOF2 modes. The dissipative role of the thermal forcings contrasts sharply with the constructive forcing due to the transient vorticity fluxes. The extent to which these thermal and vorticity forcings cancel each other will be critically examined in the following two sections.

4. Geopotential tendencies induced by eddy heat and vorticity fluxes, and by diabatic heating

a. Formulation

In this section, the quasigeostrophic geopotential tendency is used as a common measure for intercomparing the effects of different forcing mechanisms on the monthly mean circulation. The same technique has been applied by Lau and Holopainen (1984) and LN for diagnosing the transient eddy forcing in the observed atmosphere. The quasigeostrophic geopotential tendency due to eddy heat fluxes, eddy vorticity fluxes, and diabatic heating can be written in isobaric coordinates as follows (see Holton 1992, chapter 6),

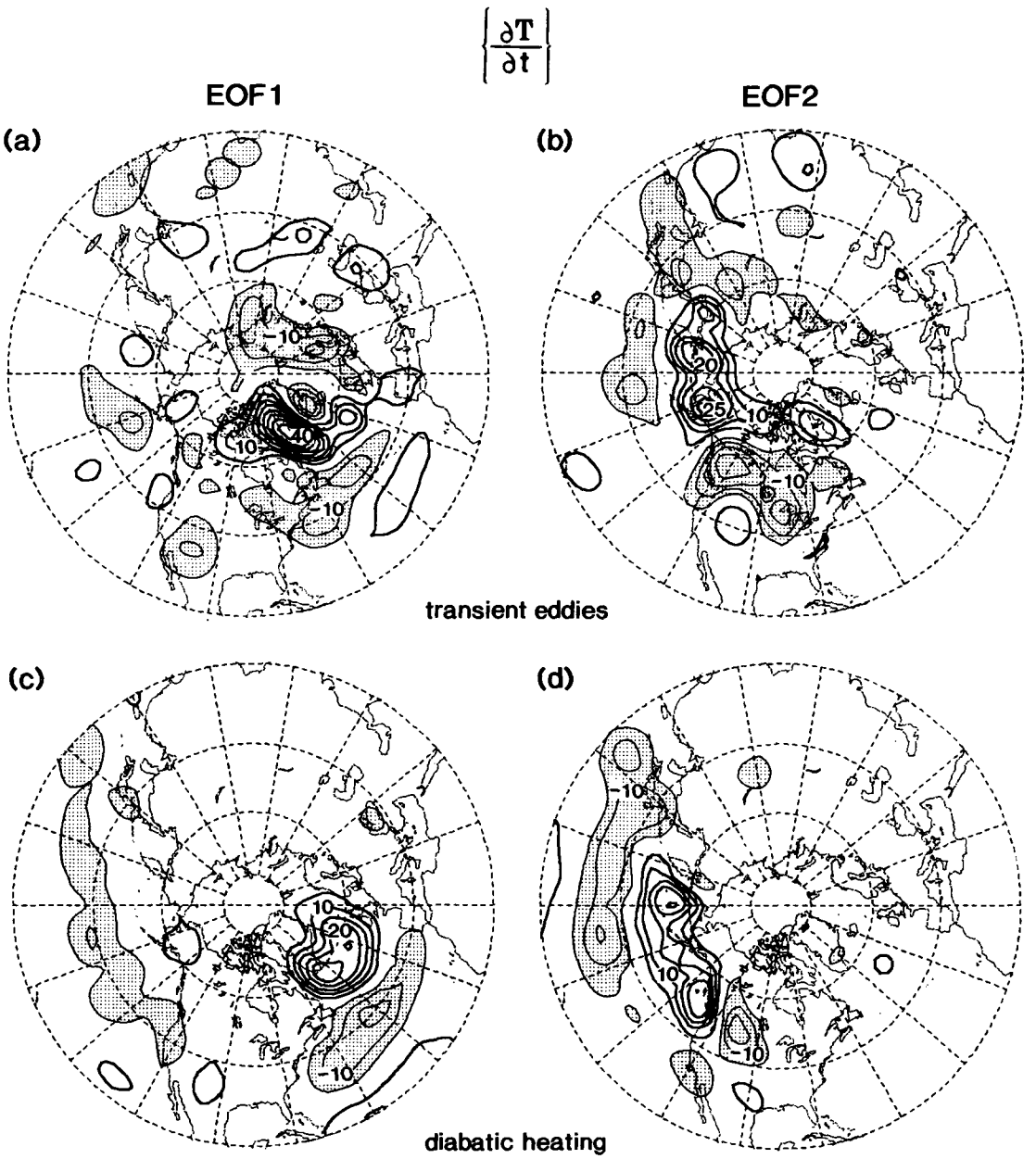

FIG. 5. Composite patterns of 830-mb temperature tendencies due to convergence of heat fluxes by all submonthly eddies (panels a, b), and to diabatic heating (panels c, d), as constructed on the basis of time coefficients for EOF1 (left panels) and EOF2 (right panels). Contour interval 5×10^{-6} K s^{-1}. Negative values less than -5×10^{-6} K s^{-1} stippled. Zero contour omitted.

$$\left\{\frac{1}{f}\nabla^2 + f\frac{\partial}{\partial p}\left(\frac{1}{\sigma}\frac{\partial}{\partial p}\right)\right\}\left(\frac{\partial \Phi}{\partial t}\right) = D_H + D_V + D_Q, \quad (1)$$

where

$$D_H = f\frac{\partial}{\partial p}\left(\frac{\nabla\cdot\overline{\mathbf{V}'\theta'}}{S}\right), \quad (2)$$

$$D_V = -(\nabla\cdot\overline{\mathbf{V}'\zeta'}), \quad (3)$$

and

$$D_Q = f\frac{\partial}{\partial p}\left\{\left(\frac{p_0}{p}\right)^{\kappa}\frac{\dot{Q}}{S}\right\} \quad (4)$$

are the forcings due to eddy heat fluxes, eddy vorticity fluxes, and diabatic heating, respectively. All symbols used above are identical to those in LN except that a new term representing diabatic heating effects (D_Q) is

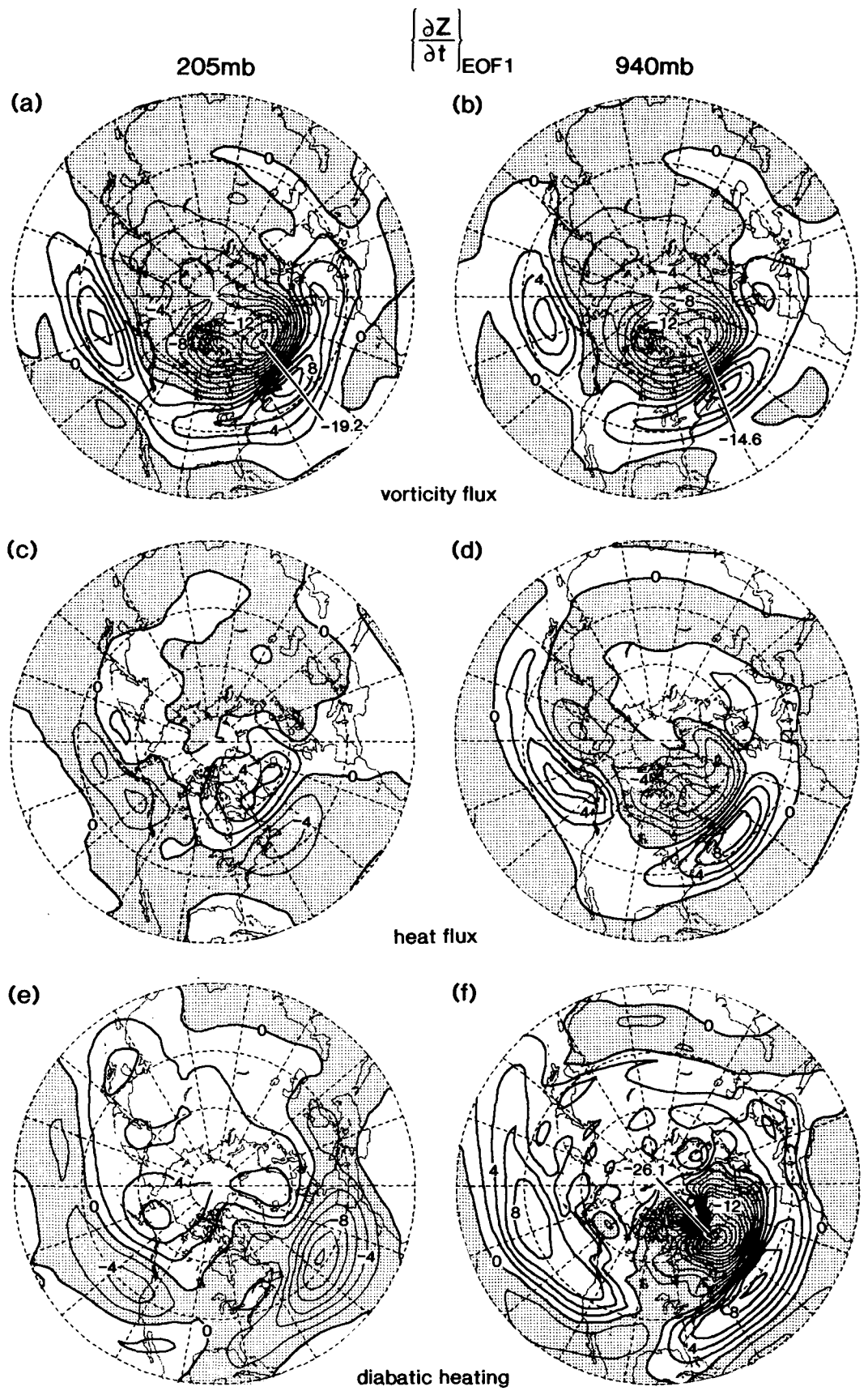
$\left\{\frac{\partial Z}{\partial t}\right\}_{EOF1}$
205mb
940mb
(a)
(b)
-19.2
-14.6
vorticity flux
(c)
(d)
heat flux
(e)
(f)
-26.1
diabatic heating

now incorporated on the right-hand side of the tendency equation (1). The numerical procedure for solving (1) for a given forcing has been described in detail by Lau and Holopainen (1984). In the present application, the solution is sought within the domain from 11.25° to 87.75°N, and from 950 to 50 mb, at intervals of 4.5° latitude and 50 mb in the meridional and vertical directions, respectively. The lower and upper boundary conditions are chosen to satisfy the thermodynamic equation with zero vertical motion. The boundary conditions at 11.25° and 87.75°N are such that the geopotential height tendency and its meridional derivative vanish locally. For each month in the 500-month sample, the height tendencies have been computed using the vorticity and heat fluxes due to synoptic eddies, as well as diabatic heating rates for that month. The eddy fluxes on isobaric surfaces have been obtained from the bandpass-filtered covariance statistics on sigma surfaces by linear interpolation.

b. *Results*

By following the same composite procedure described in section 3 (i.e., subtracting the average over those months with EOF time coefficients ranking among the bottom 10% from the average over months ranking among the top 10%), the representative patterns of the height tendency due to each type of forcing have been constructed for each EOF. Figure 6 shows the composites of height tendencies due to vorticity fluxes (a,b), heat fluxes (c,d), and diabatic heating (e,f) at 205 and 940 mb for EOF1. The corresponding results for EOF2 are shown in Fig. 7.

The patterns of the height tendencies due to synoptic eddy vorticity fluxes (top panels of Figs. 6 and 7) are again similar to those of the monthly mean height anomalies themselves (see corresponding panels in Fig. 3). The vertical structure of these height tendencies is distinctly equivalent barotropic, with the amplitude at 940 mb being slightly weaker than that at 205 mb. The 205-mb height tendency attains a maximum amplitude of about 15 m day^{-1} for both EOF composites. The time required for a forcing of this magnitude to establish the composite anomalies shown in Figs. 3a,b is approximately 18 days.

The middle panels of Figs. 6 and 7 show the height tendencies due to eddy heat fluxes. In the upper troposphere, the height tendency due to heat fluxes is opposite to, but considerably weaker than, that due to vorticity fluxes. In the lower troposphere, however, the height tendency due to heat fluxes has the same polarity and similar amplitude as that due to vorticity fluxes. Comparison with the monthly mean anomaly patterns in Fig. 3 indicates that the heat fluxes tend to destroy the upper-tropospheric monthly averaged height anomalies, and enhance the lower-tropospheric height anomalies. The height tendency examined here is seen to be in hydrostatic and thermal wind balance with the temperature tendency discussed in the previous section. In particular, it is evident that enhancements in the poleward eddy heat fluxes are accompanied by reduction of both the local meridional temperature gradient and the vertical wind shear (see also Fig. 1a of LN). By inferring the thickness and geostrophic wind tendencies from the height tendency charts in the middle panel of Figs. 6 and 7, it is seen that reduction in temperature gradient and wind shear (i.e., eastward acceleration at 940 mb, and eastward deceleration at 205 mb) indeed prevails over regions of above-normal synoptic eddy activity. The relationships among the height tendency induced by eddy vorticity fluxes, the height tendency induced by eddy heat fluxes, and the monthly mean height anomalies in the model atmosphere agree well with the observational findings presented in LN.

At 940 mb, the height tendency due to diabatic heating (Figs. 6f and 7f) exhibits some resemblance to, and is generally stronger than, the tendency due to eddy heat fluxes at the same level. The corresponding patterns compare less well at 205 mb. For both levels, the centers of extremum in the forcing associated with diabatic heating are displaced equatorward of the corresponding features in the tendency field induced by eddy heat fluxes. A similar spatial shift is also seen in the temperature tendency charts for the two types of forcings, shown in Fig. 5. This displacement is linked to the fact that, for a storm track located at a given latitude, the strongest diabatic heating resides at the same latitude, whereas the strongest eddy heat flux convergence occurs poleward of that latitude. In analogy with the discussion on the height tendency due to eddy heat fluxes, the anomalous diabatic heating also acts to reduce the meridional temperature gradient and vertical shear of the zonal wind on the equatorward flank of the site of enhanced synoptic activity.

A similar set of tendency charts has also been constructed for EOF3 and EOF4. The spatial relationships between the monthly averaged height anomalies and the forcings due to eddy fluxes and diabatic heating, as pointed out in the above discussion on Figs. 6 and 7, are also discernible in the corresponding composites for EOF3 and EOF4 (not shown).

FIG. 6. Composite patterns of quasigeostrophic height tendencies for EOF1 due to vorticity fluxes by bandpass-filtered eddies at 205 mb (a) and 940 mb (b), heat fluxes by bandpass-filtered eddies at 205 mb (c) and 940 mb (d), and diabatic heating at 205 mb (e) and 940 mb (f). Contour interval 2×10^{-5} m s^{-1}. Negative values stippled.

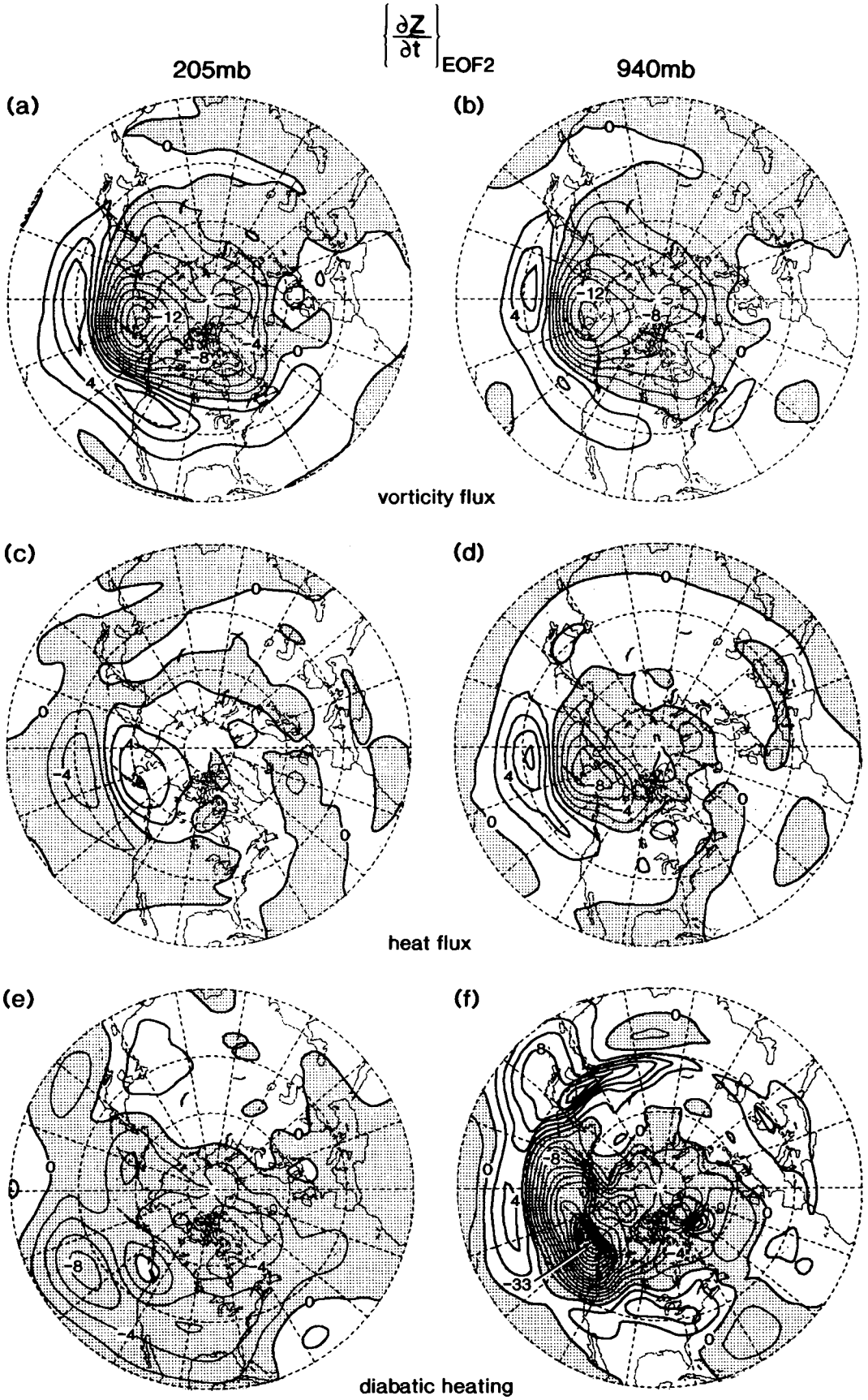

FIG. 7. Same as Fig. 6 but for EOF2.

5. Response of a linear stationary wave model to anomalous eddy fluxes and diabatic heating

a. Description of linear model

The stationary wave model used in this study is the same as that described in Ting and Held (1990). It is an exact linearization of the dry dynamical equations for the GFDL GCM described in section 2. This sigma-coordinate model includes the vorticity, divergence, thermodynamic, hydrostatic, surface pressure tendency, and continuity equations. The moisture equation in the GCM is not included in the linear model. The basic equations are linearized about a basic state. Two types of basic state have been used in this study: zonally symmetric and zonally varying. The zonally symmetric basic state has been obtained by averaging the climatological GCM data for the five-month winter season over all longitudes. The zonally varying basic state has been computed using the same GCM climatology, but with the longitudinal variations retained.

The linear model equations may be written as follows,

$$L(\mathbf{X}_0)\mathbf{X}' = \mathbf{F}' \tag{5}$$

where L is the linear operator, $\mathbf{X}_0$ the basic-state vector, $\mathbf{X}'$ the steady-state solution vector representing the monthly mean circulation anomalies, and $\mathbf{F}'$ the anomalous forcing vector. As in the GCM, all perturbation and basic-state variables are expanded using spherical harmonics. A rhomboidal truncation at wavenumber 15 is used for the model linearized about a zonally symmetric basic state, whereas a zonal wavenumber 6 and meridional wavenumber 15 truncation is utilized for the model linearized about a zonally varying basic state. The severe zonal truncation in the latter case is chosen in order to ease the computational burden. As is evident from Fig. 3, the main features of the monthly mean anomalies are rather large scale; thus, one expects the wavenumber 6 truncation to be sufficient for representing these anomalies. The linear operator L in the model also includes dissipative effects, which consist of Rayleigh friction within the planetary boundary layer in the vorticity and divergence equations, as well as a scale-selective biharmonic diffusion in the vorticity, divergence, and temperature equations. The Rayleigh friction time scale is 0.25 and 1.0 day at the lowest two model levels, $\sigma = 0.99$ and $\sigma = 0.94$, respectively. These values are chosen by linearly regressing the vertical momentum diffusion in the GCM with the corresponding boundary-layer wind. The correlation coefficient between these two fields is very high, usually above 0.9. Thus, Rayleigh friction should be a good approximation to the vertical momentum diffusion within the boundary layer of the GCM. The Rayleigh friction coefficient is set to zero at all layers above $\sigma = 0.94$. The biharmonic diffusion coefficient is chosen to be 1.0×10^{17} m^4 s^{-1}, which is 10 times stronger than that used in the GCM. A stronger diffusion serves to smooth the linear model results, but otherwise does not change the response patterns significantly. As explained in the following subsection, a thermal diffusion term is incorporated in the temperature equation, so as to represent the effects of transient eddy heat fluxes.

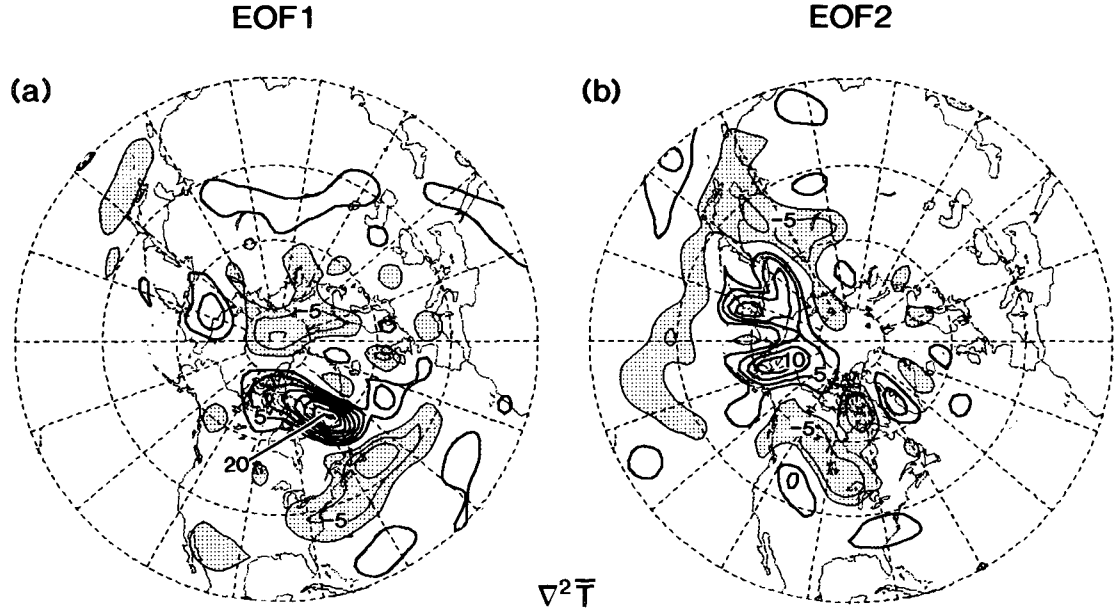

FIG. 8. Composite patterns of the Laplacian of monthly mean temperature at 830 mb, for (a) EOF1 and (b) EOF2. Contour interval 2.5×10^{-12} K m^{-2}. Negative values less than -2.5×10^{-12} K m^{-2} stippled. Zero contour omitted.

b. Parameterization of transient eddy heat fluxes

As pointed out by Branstator (1990), the linear operator L in (5), when linearized about a zonally varying time-mean state, is rather singular. This singularity is the consequence of the existence of many near-zero frequency modes. There are many ways to avoid the singularity, one of which is to increase the dissipation in the linear model. Branstator (1990) added a 10-day linear damping plus a 1000-day vertical diffusion at all levels in the vorticity, divergence, and temperature equations to avoid the singular behavior of his model.

In the present study, a thermal damping is used in the temperature equation to parameterize the effects of transient eddy heat fluxes. This strategy is mainly motivated by the tendency results presented in the previous sections, which suggest that the eddy heat transports act to reduce the local monthly mean temperature gradient. To illustrate this relationship further, the Laplacian of the composite 830-mb temperature field for EOF1 and EOF2 are presented in Fig. 8. The patterns in this figure exhibit a notable degree of resemblance with those for the eddy-induced temperature tendency (Figs. 5a,b). This favorable comparison justifies the representation of the temperature forcing due to submonthly eddies by a thermal diffusion process.

The appropriate diffusion coefficient for this heat flux parameterization may be estimated by performing a linear regression of the heat flux convergence versus the Laplacian of the monthly mean temperature. These two fields are represented by the ordinate and abscissa axes, respectively, of the scattergrams in Fig. 9, with the values of the 830-mb composite data for EOF1 (upper panel) and EOF2 (lower panel) at all model

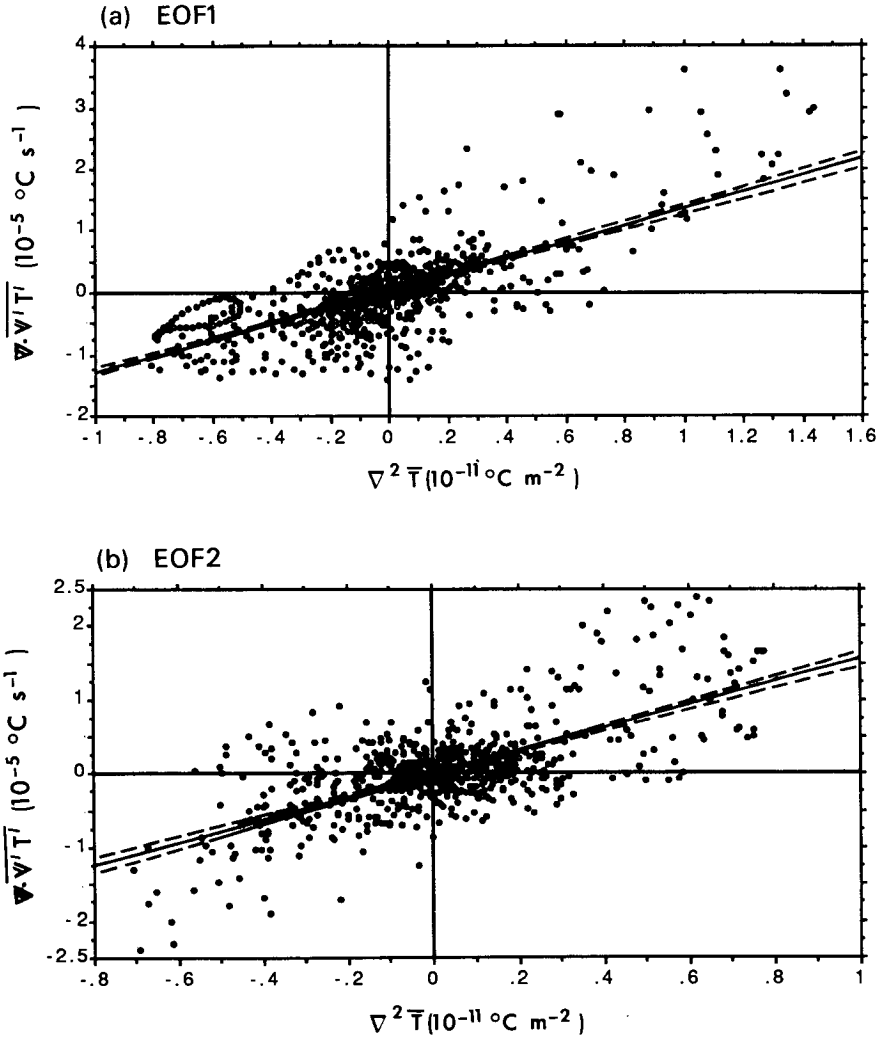

FIG. 9. Scattergram of the Laplacian of monthly mean temperature versus eddy heat flux convergence at 830 mb, as constructed using composite data of the two fields at grid points north of 20.25°N for (a) EOF1 and (b) EOF2. Shown on the same plots are the regression line, as well as lines corresponding to the 95% significance limits of the regression slope.

grid points north of 20.25°N being plotted as individual dots. Both the eddy heat flux convergence and Laplacian of temperature have been spatially smoothed by retaining the first six zonal wavenumbers. A truncation at wavenumber 15 has been used in the meridional direction. The linear regression fit between the two fields considered here (see straight lines in Fig. 9) has a slope of 1.4×10^6 (1.5×10^6) $m^2 s^{-1}$ for EOF1 (EOF2). The corresponding regression coefficients for EOF3 and EOF4 (not shown) are 1.6×10^6 and 1.7×10^6 $m^2 s^{-1}$, respectively. The spatial correlation coefficients between the two fields, which provides for a measure of the statistical significance of the regression slopes, are 0.73, 0.67, 0.74, and 0.82 for the composite data based on the four leading EOFs. Similar relationships can be found at levels other than 830 mb, with regression coefficients ranging between 1×10^6 and 1.7×10^6 $m^2 s^{-1}$. On the basis of the above analysis, a thermal diffusion coefficient of 1.5×10^6 $m^2 s^{-1}$ has been adopted at all levels in the linear model. A similar parameterization of the eddy heat fluxes has also been utilized by Ting (1991) in a linear simulation of the response of an idealized GCM to a midlatitude SST anomaly.

c. *Linear model results with zonally symmetric basic state*

In the case of a zonally symmetric basic state, the vector $\mathbf{X}_0$ in (5) is a function of latitude and height only. The anomalous forcing $\mathbf{F}'$ consists of the following: vorticity forcing due to transient vorticity fluxes; diabatic heating; and forcing due to changes in the zonally averaged basic state. When compared with the full GCM equations, it is seen that two effects are not taken into account in the present linear model framework. One is the interaction term between the zonally asymmetric component of the climatological mean flow and the zonally asymmetric component of the monthly anomalies (hereafter referred to as the linear interaction term). The other is the interaction among the monthly anomalies themselves (hereafter referred to as the nonlinear interaction term). The linear interaction term can be included in the operator linearized about a zonally varying basic state, which will be discussed in the next subsection. In the present case of a zonally symmetric basic state, the effects of the two interaction terms may be evaluated by treating them as additional forcings on the right-hand side of the linear model equations.

When linearized about a zonally symmetric basic state, the stationary wave model simulates only the zonally asymmetric component of the GCM anomaly. For a better comparison between the full GCM patterns and the linear model results, the composite GCM height anomalies at 205 mb for EOF1 and EOF2 are replotted in Figs. 10a,b, with the zonal-mean component removed. The zonally asymmetric component of the height anomalies exhibits a more wavy character when compared to the total fields (see Figs. 3a,b). The EOF1 pattern in Fig. 10a is indicative of a wave train emanating from the subtropical Atlantic, with stronger downstream signals in the Eurasian sector. Similarly, the EOF2 pattern in Fig. 10b shows a wave train extending from the central subtropical Pacific to North America. In Figs. 10c,d are shown the composite patterns of the linear model response to all anomalous forcings not incorporated in the linear operator (i.e., eddy vorticity fluxes, diabatic heating, effect due to changes in the basic state, and linear and nonlinear interactions), for EOF1 and EOF2, respectively. If the dissipation applied in the linear model were identical to that used in the GCM, one would expect the linear model to reproduce exactly the full GCM patterns in Figs. 10a,b. Indeed, there are only minor differences between the GCM patterns and the linear model solutions. Such differences are mainly due to the approximations made in treating vertical momentum diffusion and transient eddy heat fluxes in the linear model. The difference in the biharmonic diffusion coefficient used in the GCM and the linear model plays a minor role. The good resemblance between the full GCM anomalies and the linear model solutions indicates that the effects of the eddy heat fluxes are well represented by the thermal diffusion mechanism described in the previous subsection.

In order to assess the impact of the linear interaction term on the linear model response, Eq. (5) has also been solved with this term being taken out from the anomalous forcing on the right-hand side. The solutions thus obtained are shown in Figs. 10e,f. The detailed structure of the wave trains in the latter patterns is quite different from that in the full GCM anomalies. The noticeable deterioration of the linear model solution in the absence of the linear interaction term clearly demonstrates the necessity of incorporating the zonally varying component of the climatological flow field in the basic state. A similar conclusion has been reached by Branstator (1992) in his diagnosis of low-frequency anomalies appearing in the NCAR Community Climate Model.

d. *Linear model results with a zonally asymmetric basic state*

In recognition of the importance of the effects of the linear interaction terms, our attention will henceforth be focused on the linear model solutions for a zonally asymmetric basic state (hereafter referred to as the wavy linear model). In the present case, the linear model is configured such that both the zonal mean and the zonally asymmetric components can be obtained from the solution. Both the linear interaction terms and the effect due to changes in the zonal-mean basic state, which are specified as explicit forcing in the case with a zonally

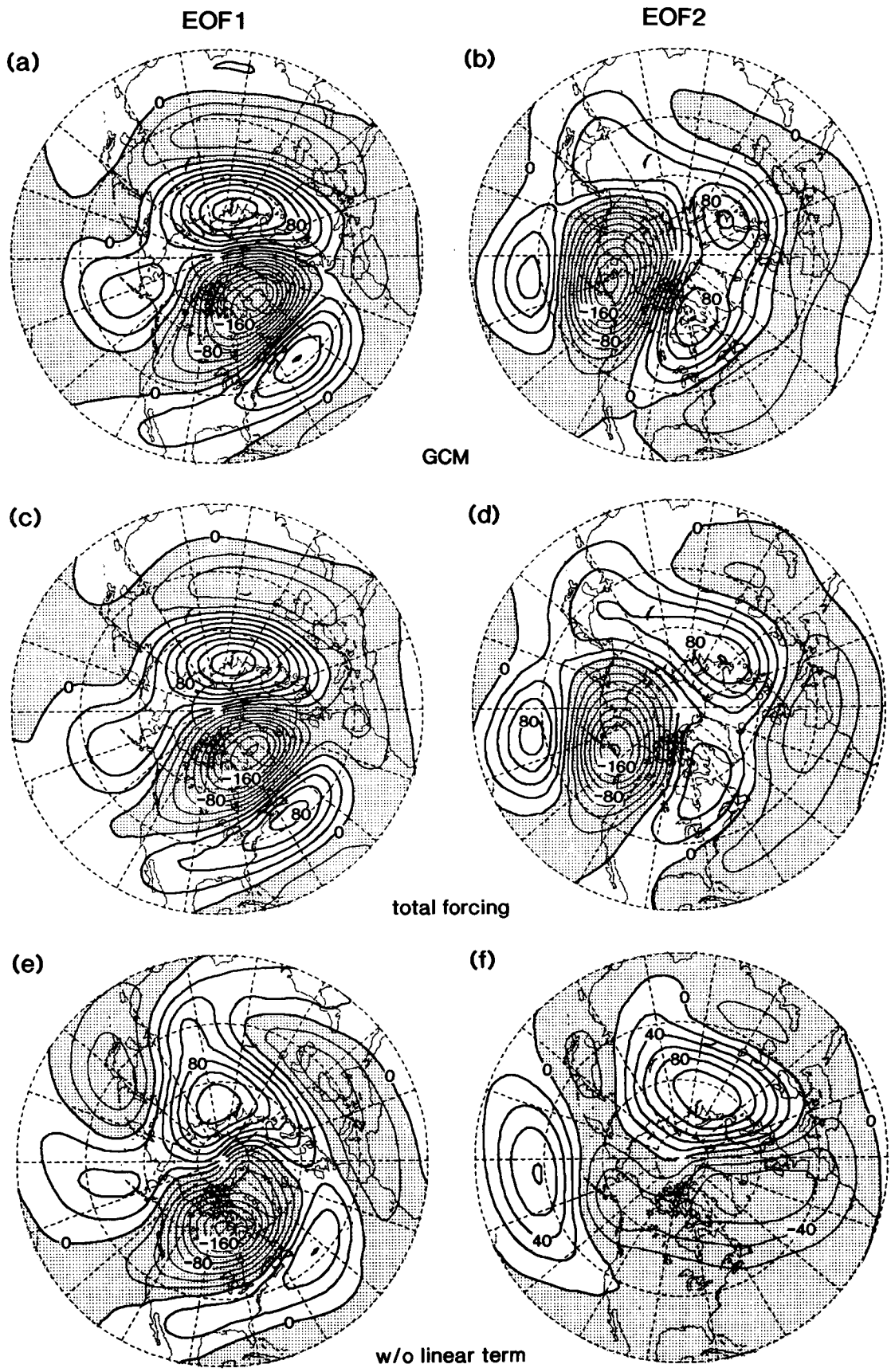
EOF1
EOF2
(a)
(b)
GCM
(c)
(d)
total forcing
(e)
(f)
w/o linear term

symmetric basic state, are now incorporated in the wavy linear operator. The explicit forcing terms for the wavy linear model include the convergence of eddy vorticity fluxes, diabatic heating, and the nonlinear interaction terms.

In conformity with the presentation in the previous subsection, we shall devote our attention to the zonally asymmetric component of the wavy linear model solution. The composite 205-mb height patterns of the wavy linear model response to total forcing are displayed in Figs. 11a,b. By comparing these solutions with the corresponding GCM patterns in Figs. 10a,b, one finds that the wavy linear model provides a good simulation of the GCM monthly mean anomalies. The dipoles over the North Atlantic and North Pacific are well captured and the wave trains are reproduced by the wavy linear model. The solution of the wavy linear model at 940 mb (not shown) is similar in spatial structure to that at 205 mb, but with about half of its amplitude. There are, however, some minor differences between the linear model results and the GCM patterns. The linear solution for EOF1 has a weaker amplitude than that of the GCM counterpart. The weak low center near 30°, 150°E in Fig. 11b is not present in the GCM pattern in Fig. 10b. These differences may be accounted for by the more severe zonal wave truncation of the wavy linear model, and the fact that the zonal-mean anomaly (not shown) is not very well simulated by the wavy linear model. There could also be influences of the near-resonant modes (see discussion in section 5e).

The contributions by individual forcing mechanisms to the total solution of the wavy linear model at 205 mb are also shown in Fig. 11, with panels c, d illustrating the effects of eddy vorticity fluxes, panels e, f the effects of diabatic heating, and panels g, h the impact of nonlinear interactions. For EOF2, the wave train forced by vorticity fluxes alone (Fig. 11d) is very similar to the response to total forcing (Fig. 11b), with the amplitude of the wave train being somewhat stronger in the response to eddy vorticity transports alone. The principal features in Fig. 11d are also discernible in the wavy linear model response to diabatic heating (Fig. 11f), with the latter pattern having a reversed polarity and weaker amplitudes. Hence, the diabatic processes tend to partially offset the effects of the vorticity transients. For EOF1, the wavy linear model response to eddy vorticity forcing (Fig. 11c) bears some resemblance to the total solution (Fig. 11a) in much of the North American, Atlantic, and Eurasian sectors. However, notable discrepancies between Figs. 11a and 11c are seen over the Pacific basin, where the effects of diabatic heating (Fig. 11e) appear to contribute significantly to the total forcing. For both EOF1 and EOF2, the vertical structure of the response to either transient vorticity forcing or diabatic heating is equivalent barotropic, with the solution at 940 mb (not shown) being considerably weaker than but qualitatively similar to that at 205 mb. The impact of the nonlinear interaction term is generally small when compared to the other forcings. For EOF1, the nonlinear effects force a weak pattern (Fig. 11g) that bears some spatial resemblance to the total solution (Fig. 11a).

The conclusions drawn from the above diagnosis of the GCM anomalies using a wavy linear model are in general accord with the findings based on the tendency calculations presented in section 4. Of particular interest is that both the tendency method and the linear steady-state response indicate the dominant role of the vorticity transients in forcing the monthly mean circulation anomalies throughout the troposphere. Another point worth noting here is that, in the upper troposphere, the dissipative role of diabatic heating, as suggested by the tendency results, is even more evident in the wavy linear model solutions.

The wavy linear model solutions in Figs. 11c,d have been obtained using vorticity flux data for eddies with periods ranging from a day to a month (i.e., the submonthly eddies). The corresponding solutions for synoptic-scale fluctuations, as computed using bandpass-filtered eddy statistics, are shown in Fig. 12. Comparison of the latter patterns with those in Figs. 11c,d indicates that the synoptic eddies account for approximately half of the linear response to transient vorticity forcing for all submonthly time scales. This finding is consistent with the tendency calculations presented in Fig. 4.

The wavy linear model does not provide a satisfactory simulation of the EOF3 pattern. Although the spatial structure of the wavy linear model solution is similar to the full GCM pattern, the amplitude of the wavy model response to the total forcing for EOF3 is only about one-third of that in the GCM composite. Whether this failure is related to the resonance of the wavy linear model is not clear. On the other hand, the wavy linear model yields a reasonable simulation of the EOF4 pattern. Preliminary examination of the spatial correlation between streamfunction tendency due to transient vorticity transport and the streamfunction anomaly itself reveals a less coherent rela-

FIG. 10. Composite patterns of the zonally asymmetric component of the geopotential height at 205 mb, for the full GCM (panels a, b), response of linear model with zonally symmetric basic state to vorticity transients, diabatic heating, effect due to changes in zonal-mean zonal flow, linear and nonlinear interaction terms (panels c, d), and response to vorticity transients, diabatic heating, and effect due to changes in zonal-mean zonal flow (panels e, f), as constructed on the basis of the time coefficients for EOF1 (left panels) and EOF2 (right panels). Contour interval 20 m. Negative values stippled.

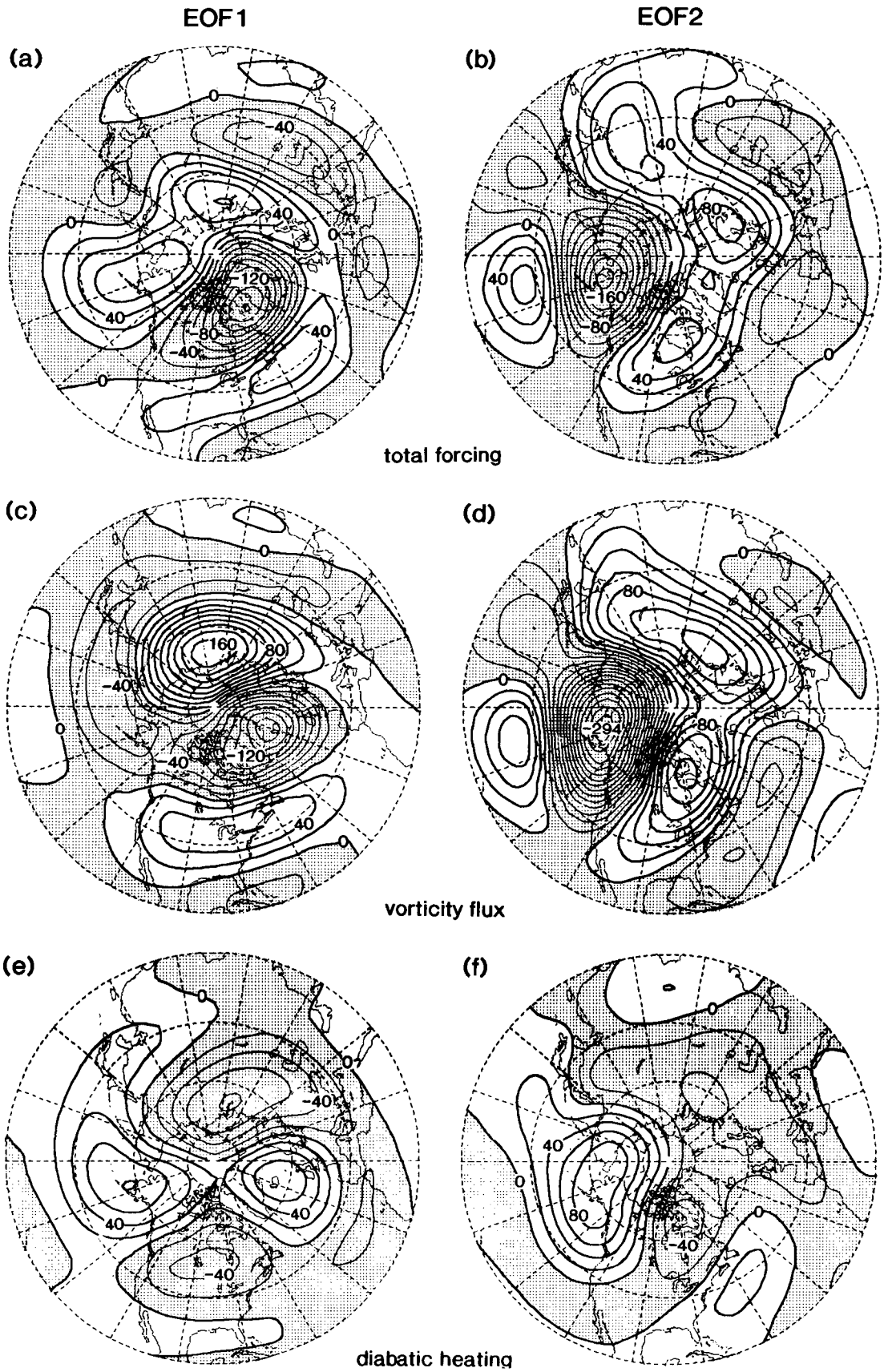
EOF1
EOF2
(a)
(b)
total forcing
(c)
(d)
vorticity flux
(e)
(f)
diabatic heating

FIG. 11.

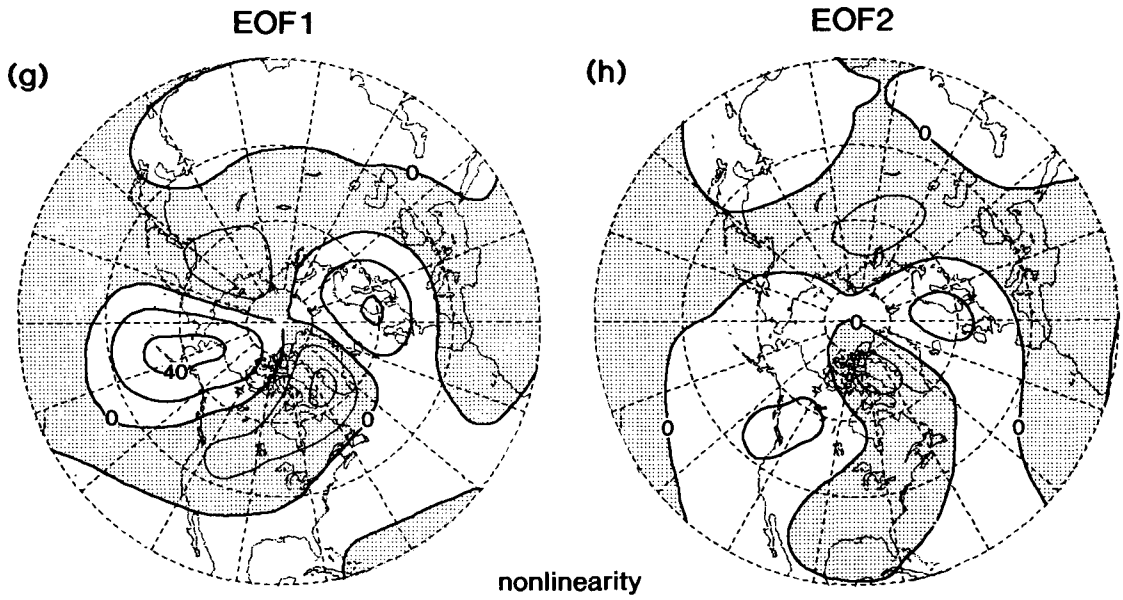

FIG. 11. Composite patterns of the zonally asymmetric component of the geopotential height at 205 mb in the wavy linear model response to vorticity transients, diabatic heating, and nonlinearity (panels a, b), response to vorticity transients only (panels c, d), response to diabatic heating only (panels e, f), and response to nonlinearity only (panels g, h), as constructed on the basis of the time coefficients for EOF1 (left panels) and EOF2 (right panels). Contour interval 20 m. Negative values stippled.

tionship for EOF3 in comparison to other EOFs, thus suggesting that mechanisms other than eddy forcing may be contributing to this particular mode.

e. Impact of the wave amplitude of the basic state

As was mentioned in section 5b, the operator L for the model linearized about a zonally varying climatological flow is rather singular. It is hence important to investigate the impact of near-resonant modes associated with this singularity on the linear solutions presented in section 5d. This issue is addressed by exploring the relationship between the degree of the waviness of the basic state and the wavy linear model response to the vorticity transients. When there is no

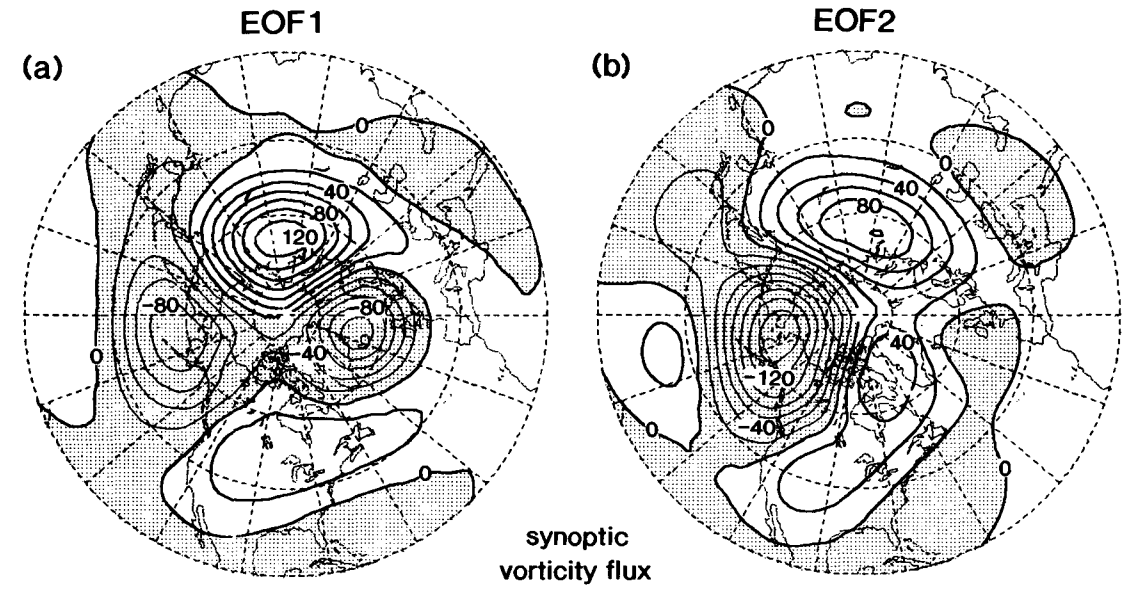

FIG. 12. Composite patterns of the zonally asymmetric component of the geopotential height at 205 mb in the wavy linear model response to bandpass-filtered vorticity transients, for EOF1 (a), EOF2 (b). Contour interval 20 m. Negative values stippled.

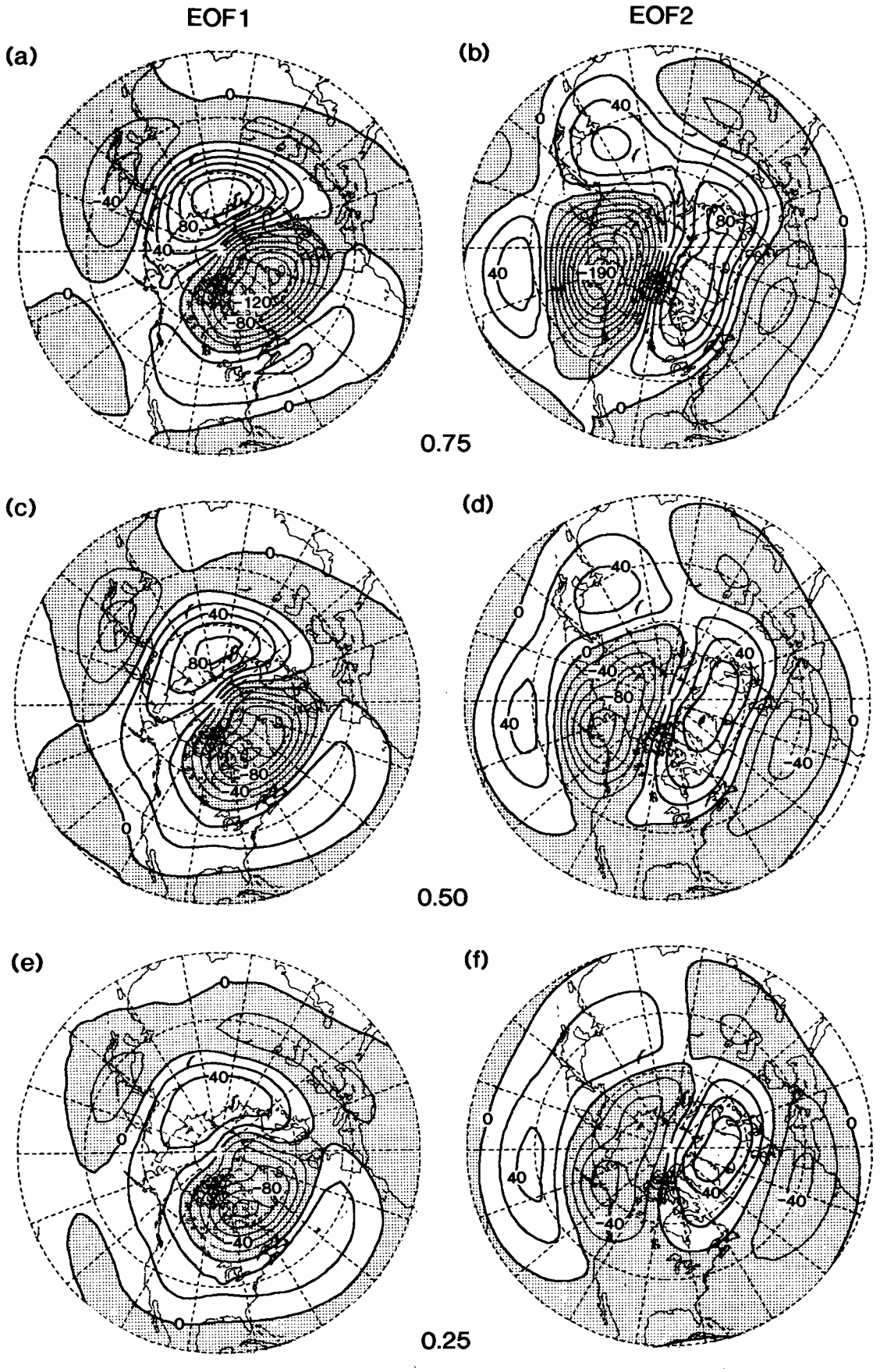
EOF1
EOF2
(a)
(b)
(c)
(d)
(e)
(f)
0.75
0.50
0.25

longitudinal dependence in the background flow, the solution of the wavy linear model would degrade to the linear model with zonally symmetric basic state (see section 5c). In the opposite extreme, when the full wave amplitude of the climatological flow is incorporated in the basic state, the wavy linear model would yield the solution described in section 5d. Several basic states between these two extremes have been constructed by adding a certain fraction of the amplitude of the zonally asymmetric background flow to the zonally symmetric circulation. Figure 13 shows the linear model responses to the vorticity transients for some of the latter basic states. The fraction of the climatological wave amplitude being retained in these intermediate basic states varies from 0.75 (top panels), to 0.50 (middle panels), and to 0.25 (bottom panels). Model solutions for both EOF1 (left) and EOF2 (right) are displayed. The solutions corresponding to a weak wavy basic state (Figs. 13e and 13f) are similar to those obtained using a zonally symmetric basic state (not shown). The amplitude of the height anomalies in Fig. 13 increases smoothly as the degree of waviness of the basic state is enhanced. The spatial patterns of the linear solutions, however, remain the same in all three cases. Judging from the absence of any abrupt changes in amplitude and spatial pattern as the degree of waviness of the basic state is increased, it is unlikely that resonance plays a significant role in the linear solutions with wavy mean states, at least for the first two EOF patterns.

6. Conclusions

The month-to-month variability in a 100-year GCM experiment with fixed climatological SST conditions has been analyzed. The long duration of the GCM dataset and the availability of a full range of atmospheric fields (such as diabatic heating) allows for a more complete and internally consistent diagnosis than is possible with the observational records. For all the leading modes of variability, fluctuations in the monthly mean circulation are seen to be accompanied by systematic changes in the diabatic heating field, as well as vorticity and heat transports by eddies with submonthly time scales. The quasigeostrophic height tendency due to eddy vorticity fluxes reinforces the monthly mean height anomalies at all tropospheric levels. In contrast, the eddy-induced height tendency due to heat fluxes has opposite polarities in the upper and lower troposphere: it offsets the monthly mean height anomaly in the upper troposphere, and reinforces the monthly mean anomaly in the lower troposphere. In the upper troposphere, the constructive effect of vorticity fluxes is stronger than the dissipative effect of heat fluxes. Thus, the net effect of the transient eddies is to maintain the monthly mean height anomalies throughout the troposphere. Similar relationships between the monthly mean anomaly and the eddy-induced height tendencies have been reported in the observational studies by Lau (1988) and LN. This agreement between observational and model results suggests that similar mechanisms may be at work in sustaining the monthly mean anomalies in the real and simulated atmospheres. In the upper troposphere, the diabatic heating tends to offset the monthly mean anomalies, but the spatial pattern of the heating-induced height tendency is not exactly opposite to the height anomaly itself. In the lower troposphere, the height tendency due to heating is similar to the tendency induced by heat fluxes, but twice as strong.

In parallel with the quasigeostrophic tendency computations, the nature of the simulated monthly mean height anomalies has been diagnosed using a linear stationary wave model. In view of the tendency of the eddy heat fluxes to reduce the local monthly mean temperature gradient, the effects of these fluxes have been parameterized as a diffusion term in the temperature equation. When linearized about a zonally symmetric basic state and forced by vorticity transients, heating, and effect due to changes in the basic state, the stationary wave model does not provide a satisfactory simulation of the full GCM anomalies. This model is able to reproduce the full GCM patterns only when the linear interaction between the climatological waves and the anomalous flow has been included as an additional forcing, thus indicating the importance of incorporating the zonally asymmetric component of the model climatology in the basic state. This finding motivated us to use a model linearized about the three-dimensional time mean flow. The latter model yields a good simulation of the two leading patterns of monthly variability in the GCM experiment. By considering the effects of vorticity transients and diabatic heating separately, it is found that the transient vorticity forcing plays a constructive role throughout the troposphere, and the diabatic heating acts to partially offset the eddy vorticity forcing in the upper troposphere.

The key findings of the tendency method are largely in accord with those based on linear modeling. Among the various forcing mechanisms considered here, the constructive effects of the eddy vorticity fluxes appear to be the most significant. The time mean, zonally asymmetric component of the basic state also plays an important role. These stationary waves coexist with

FIG. 13. Composite patterns of the zonally asymmetric component of the geopotential height at 205 mb in the wavy linear model response to vorticity transients, when the basic state retains 0.75 (panels a, b), 0.5 (panels c, d), and 0.25 (panels e, f) of the full wave amplitude of the GCM climatology, as constructed on the basis of the time coefficients for EOF1 (left panels) and EOF2 (right panels). Contour interval 20 m. Negative values stippled.

well-defined storm tracks in certain longitudinal sectors; they also lead to enhancements of the response to anomalous forcing through wave–wave interaction. The usefulness of the linear model currently in use for diagnosing various anomalous patterns is somewhat limited due to the presence of near-resonance modes. However, the impact of these modes on the monthly mean anomalies seems to be rather weak. One possible way to overcome this model defect is the development of a fully nonlinear stationary wave model.

A full understanding of the origin and maintenance of low-frequency atmospheric variability requires deeper theoretical insights on the mutual interactions between monthly mean anomalies, high-frequency transients, and the zonally varying background flow. The nature of such interactions has been studied extensively in simple two-layer models (Reinhold and Pierrehumbert 1982; Vautard and Legras 1988) and a barotropic model (Shutts 1983). In accord with the findings presented here, these simple models also indicate that the coexistence of higher-frequency transients and the large-scale flow leads to preferred modes of low-frequency fluctuations. The high spatial correlation between the streamfunction tendency due to transient vorticity flux convergences and the monthly anomalies (compare Fig. 4 with Figs. 3a,b) suggests a strong link between the two quantities. If it is feasible to parameterize the transient vorticity forcing in terms of large-scale low-frequency fluctuations, either in a linear or nonlinear manner, then there would be no dominant explicit forcing in the physical system under consideration. The low-frequency fluctuations could then be viewed as either preferred stationary eigenmodes of the zonally varying climatological flow with the linear feedback from the transients included (Branstator, personal communication), or free oscillations of the nonlinear system due to nonlinearities in the parameterization of the high-frequency transients. At the present time, we do not yet understand the link between high- and low-frequency transients well enough to actually parameterize the effect of the high-frequency vorticity transport. Future work is obviously needed along this direction.

Acknowledgments. We would like to thank Isaac Held and Grant Branstator for many stimulating discussions on this work. We are indebted to Mary Jo Nath, who carried out the GCM experiment described here, and assisted in the analysis phase of this endeavor. Isaac Held, Hisashi Nakamura, Randy Dole, Jeff Anderson, and two anonymous reviewers have made helpful comments on earlier drafts of this manuscript. Clara Deser kindly helped us in producing the regression charts in Fig. 9. The Scientific Illustration Group at GFDL assisted in the preparation of the figures. This work is supported by the NOAA Climate and Global Change Program.

REFERENCES

Anderson, J. L., 1991: The robustness of barotropic unstable modes in a zonally varying atmosphere. *J. Atmos. Sci.*, **48,** 2393–2410.

Barnston, A. G., and R. E. Livezey, 1987: Classification, seasonality and persistence of low-frequency atmospheric circulation patterns. *Mon. Wea. Rev.*, **115,** 1083–1126.

Blackmon, M. L., and N.-C. Lau, 1980: Regional characteristics of the northern hemisphere wintertime circulation: A comparison of the simulation of a GFDL general circulation model with observations. *J. Atmos. Sci.*, **37,** 497–514.

——, J. E. Geisler, and E. J. Pitcher, 1983: A general circulation model study of January climate anomaly patterns associated with the interannual variation of equatorial sea-surface temperatures. *J. Atmos. Sci.*, **40,** 1410–1425.

——, Y. H. Lee, and J. M. Wallace, 1984a: Horizontal structure of 500 mb height fluctuations with long, intermediate and short time scales. *J. Atmos. Sci.*, **41,** 961–979.

——, ——, ——, and H. H. Hsu, 1984b: Time variation of 500 mb height fluctuations with long, intermediate and short time scales as deduced from lag-correlation statistics. *J. Atmos. Sci.*, **41,** 981–991.

Branstator, G. W., 1985a: Analysis of general circulation model sea-surface temperature anomaly simulations using a linear model. Part I: Forced solutions. *J. Atmos. Sci.*, **42,** 2225–2241.

——, 1985b: Analysis of general circulation model sea-surface temperature anomaly simulations using a linear model. Part II: eigenvalue problems. *J. Atmos. Sci.*, **42,** 2225–2241.

——, 1990: Low-frequency patterns induced by stationary waves. *J. Atmos. Sci.*, **47,** 629–648.

——, 1992: The maintenance of low-frequency atmospheric anomalies. *J. Atmos. Sci.*, **49,** 1924–1945.

Esbenson, S. K., 1984: A comparison of intermonthly and interannual teleconnections in the 700 mb geopotential height field during the Northern Hemisphere winter. *Mon. Wea. Rev.*, **112,** 2016–2032.

Geisler, J. E., M. L. Blackmon, G. T. Bates, and S. Munoz, 1985: Sensitivity of January climate response to the magnitude and position of equatorial Pacific sea surface temperature anomalies. *J. Atmos. Sci.*, **42,** 1037–1049.

Gordon, C. T., and W. F. Stern, 1982: A description of the GFDL global spectral model. *Mon. Wea. Rev.*, **110,** 625–644.

Held, I. M., S. W. Lyons, and S. Nigam, 1989: Transients and the extratropical response to El Niño. *J. Atmos. Sci.*, **46,** 163–174.

Holton, J. R., 1992: *An Introduction to Dynamical Meteorology,* third ed. Academic Press, 511pp.

Horel, J. D., 1981: A rotated principle component analysis of the interannual variability of the Northern Hemisphere 500 mb height field. *Mon. Wea. Rev.*, **109,** 2080–2092.

——, and J. M. Wallace, 1981: Planetary-scale atmospheric phenomena associated with the Southern Oscillation. *Mon. Wea. Rev.*, **109,** 813–829.

Hoskins, B. J., and D. J. Karoly, 1981: The steady linear response of a spherical atmosphere to thermal and orographic forcing. *J. Atmos. Sci.*, **38,** 1179–1196.

Hsu, H-H., and J. M. Wallace, 1985: Vertical structure of wintertime teleconnection patterns. *J. Atmos. Sci.*, **42,** 1693–1710.

Klein, W. H., 1983: Objective specification of monthly mean surface temperature from mean 700 mb heights. *Mon. Wea. Rev.*, **111,** 674–691.

Kushnir, Y., and N.-C. Lau, 1992: The general circulation model response to a north Pacific SST anomaly: dependence on time scale and pattern polarity. *J. Climate,* **5,** 271–283.

Kutzbach, J. E., 1970: Large-scale features of monthly mean Northern Hemisphere anomaly maps of sea-level pressure. *Mon. Wea. Rev.*, **98,** 708–716.

Lau, N.-C., 1981: A Diagnostic study of recurrent meteorological anomalies appearing in a 15-year simulation with a GFDL general circulation model. *Mon. Wea. Rev.*, **109,** 2287–2311.

——, 1985: Modelling the seasonal dependence of the atmospheric

response to observed El Niños in 1962–76. *Mon. Wea. Rev.*, **113,** 1970–1996.

——, 1988: Variability of the observed mid-latitude storm tracks in relation to low-frequency changes in the circulation pattern. *J. Atmos. Sci.*, **45,** 2718–2743.

——, and E. O. Holopainen, 1984: Transient eddy forcing of the time-mean flow as identified by geopotential tendencies. *J. Atmos. Sci.*, **41,** 313–328.

——, and M. J. Nath, 1991: Variability of the baroclinic and barotropic transient eddy forcing associated with monthly changes in the midlatitude storm tracks. *J. Atmos. Sci.*, **48,** 2589–2613.

Manabe, S., D. G. Hahn, and J. L. Holloway, 1979: Climate simulation with GFDL spectral models of the atmosphere. GARP Publ. Ser. No.22, WMO, Geneva.

Mullen, S. L., 1987: Transient eddy forcing of blocking flows. *J. Atmos. Sci.*, **44,** 3–22.

Nigam, S., I. M. Held, and S. W. Lyons, 1986: Linear simulation of the stationary eddies in a general circulation model. Part I: The no-mountain model. *J. Atmos. Sci.*, **43,** 2944–2961.

——, ——, and ——, 1988: Linear simulation of the stationary eddies in a general circulation model. Part II: The mountain model. *J. Atmos. Sci.*, **45,** 1433–1452.

Reinhold, B. B., and R. T. Pierrehumbert, 1982: Dynamics of weather regimes: Quasi-stationary waves and blocking. *Mon. Wea. Rev.*, **110,** 1105–1145.

Schubert, S., C.-K. Park, W. Higgins, S. Moorthi, and M. Suarez, 1990a: An atlas of ECMWF analyses (1980–87). Part I—First moment quantities. NASA Tech. Memo. 100747. 273pp.

——, W. Higgins, C.-K. Park, S. Moorthi, and M. Suarez, 1990b: An atlas of ECMWF analyses (1980–87). Part II—second moment quantities. NASA Tech. Memo. 100762. 286pp.

Shukla, J., and J. M. Wallace, 1983: Numerical simulation of the atmospheric response to equatorial Pacific sea surface temperature anomalies. *J. Atmos. Sci.*, **40,** 1613–1630.

Shutts, G. J., 1983: The propagation of eddies in diffluent jetstreams: eddy vorticity forcing of "blocking" flow fields. *Quart. J. Roy. Meteor. Soc.*, **109,** 737–761.

Simmons, A. J., 1982: The forcing of stationary wave motion by tropical diabatic heating. *Quart. J. Roy. Meteor. Soc.*, **108,** 503–534.

——, J. M. Wallace, and G. W. Branstator, 1983: Barotropic wave propagation and instability, and atmospheric teleconnection patterns. *J. Atmos. Sci.*, **40,** 1363–1392.

Ting, M., 1991: The stationary wave response to a midlatitude SST anomaly in an idealized GCM. *J. Atmos. Sci.*, **48,** 1249–1275.

——, and I. M. Held, 1990: The stationary wave response to a tropical SST anomaly in an idealized GCM. *J. Atmos. Sci.*, **47,** 2546–2566.

van Loon, H., and J. C. Rogers, 1978: The seesaw in winter temperatures between Greenland and northern Europe. Part I: General description. *Mon. Wea. Rev.*, **106,** 296–310.

Vautard, R., and B. Legras, 1988: On the source of midlatitude low-frequency variability. Part II: Nonlinear equilibration of weather regimes. *J. Atmos. Sci.*, **45,** 2845–2867.

Walker, G. T., and E. W. Bliss, 1932: World Weather V. *Mem. Roy. Meteor. Soc.*, **4,** 53–84.

Wallace, J. M., and D. S. Gutzler, 1981: Teleconnections in the geopotential height field during the Northern Hemisphere winter. *Mon. Wea. Rev.*, **109,** 784–812.

Zhang, Z., 1988: The linear study of zonally asymmetric barotropic flows. Ph.D. thesis, University of Reading, 169 pp.